



National Library  
of Canada

Bibliothèque nationale  
du Canada

Canadian Theses Service

Services des thèses canadiennes

Ottawa, Canada  
K1A 0N4

## CANADIAN THESES

## THÈSES CANADIENNES

### NOTICE

The quality of this microfiche is heavily dependent upon the quality of the original thesis submitted for microfilming. Every effort has been made to ensure the highest quality of reproduction possible.

If pages are missing, contact the university which granted the degree.

Some pages may have indistinct print especially if the original pages were typed with a poor typewriter ribbon or if the university sent us an inferior photocopy.

Previously copyrighted materials (journal articles, published tests, etc.) are not filmed.

Reproduction in full or in part of this film is governed by the Canadian Copyright Act, R.S.C. 1970, c. C-30.

### AVIS

La qualité de cette microfiche dépend grandement de la qualité de la thèse soumise au microfilmage. Nous avons tout fait pour assurer une qualité supérieure de reproduction.

S'il manque des pages, veuillez communiquer avec l'université qui a conféré le grade.

La qualité d'impression de certaines pages peut laisser à désirer, surtout si les pages originales ont été dactylographiées à l'aide d'un ruban usé ou si l'université nous a fait parvenir une photocopie de qualité inférieure.

Les documents qui font déjà l'objet d'un droit d'auteur (articles de revue, examens publiés, etc.) ne sont pas microfilmés.

La reproduction, même partielle, de ce microfilm est soumise à la Loi canadienne sur le droit d'auteur, S.R.C. 1970, c. C-30.

**THIS DISSERTATION  
HAS BEEN MICROFILMED  
EXACTLY AS RECEIVED**

**LA THÈSE A ÉTÉ  
MICROFILMÉE TELLE QUE  
NOUS L'AVONS REÇUE**

THE UNIVERSITY OF ALBERTA

Computer Modelling of Water Droplet Trajectories in An  
Axi-symmetric Wind Tunnel Contraction

by

Wing Ho Lam

(C)

A THESIS

SUBMITTED TO THE FACULTY OF GRADUATE STUDIES AND RESEARCH  
IN PARTIAL FULFILMENT OF THE REQUIREMENTS FOR THE DEGREE  
OF Master of Science

Department of Mechanical Engineering

EDMONTON, ALBERTA

FALL 1986

Permission has been granted to the National Library of Canada to microfilm this thesis and to lend or sell copies of the film.

The author (copyright owner) has reserved other publication rights, and neither the thesis nor extensive extracts from it may be printed or otherwise reproduced without his/her written permission.

L'autorisation a été accordée à la Bibliothèque nationale du Canada de microfilmer cette thèse et de prêter ou de vendre des exemplaires du film.

L'auteur (titulaire du droit d'auteur) se réserve les autres droits de publication; ni la thèse ni de longs extraits de celle-ci ne doivent être imprimés ou autrement reproduits sans son autorisation écrite.

ISBN 0-315-32314-0

THE UNIVERSITY OF ALBERTA

RELEASE FORM

NAME OF AUTHOR Wing Ho Lam  
TITLE OF THESIS Computer Modelling of Water Droplet  
Trajectories in An Axi-symmetric Wind  
Tunnel Contraction  
DEGREE FOR WHICH THESIS WAS PRESENTED Master of Science  
YEAR THIS DEGREE GRANTED FALL 1986

Permission is hereby granted to THE UNIVERSITY  
OF ALBERTA LIBRARY to reproduce single copies of  
this thesis and to lend or sell such copies for  
private, scholarly or scientific research purposes  
only.

The author reserves other publication rights,  
and neither the thesis nor extensive extracts from  
it may be printed or otherwise reproduced without  
the author's written permission.

(SIGNED) *Wing Ho Lam*.....

PERMANENT ADDRESS:

9407 - 52 Street

Edmonton, Alberta.

T6B 1G5

DATED *July 18*.....1986

THE UNIVERSITY OF ALBERTA  
FACULTY OF GRADUATE STUDIES AND RESEARCH

The undersigned certify that they have read, and recommend to the Faculty of Graduate Studies and Research, for acceptance, a thesis entitled Computer Modelling of Water Droplet Trajectories in An Axi-symmetric Wind Tunnel Contraction submitted by Wing Ho Lam in partial fulfilment of the requirements for the degree of Master of Science.

.....*EM Jates*.....

Supervisor

.....*Roger W. Torgood*.....

.....*Edward W. Brown*.....

Date.....*July 4, 1986*.....

## ABSTRACT

A computer program, written in FORTRAN language, was developed to model the flow inside any test facility with an axi-symmetric cross section. The flow field limited to the case of incompressible potential flow was calculated by using the exact solution of the Neumann problem. Also developed was a program which estimates the thermodynamic and dynamic properties of water droplets passing through this type of test facility. This allows both the temperature and the velocity of the droplets to be predicted. The gravitational effect on the droplet was included in the equations of motion. Using these equations of motion in a three-dimensional model allows the location of the water droplets to be determined and the trajectory of the droplets to be recorded.

A parametric study has been performed on the FROST icing wind tunnel of the Mechanical Engineering Department at the University of Alberta. It was found that thermodynamic and dynamic equilibrium are achieved with the free stream for 10 micron diameter water droplets up to a test section speed of 50 m/s. However, for bigger droplets (50 microns and 100 microns) both equilibrium were not possible even at test section speed of 25 m/s.

The performance of two wind tunnels of markedly different contraction shapes were compared. The results showed that a gently sloping contraction is a better shape

for providing thermodynamic equilibrium for the droplets,  
while a steeper contraction is a better shape for dynamic  
equilibrium.

### Acknowledgements

I wish to express my deep appreciations to Dr. E.M. Gates who supervised my study and assisted in the preparation of this thesis, and for his patience and support throughout the course of the work.

I would also like to extend my thanks to both Mr. G. McEwen and Mr. R. Narten for helping to proof read the initial drafts of the thesis. Thanks are also extended to Mr. E. Leung for helping to arrange for the production of the final copies of this thesis.

Funding for this project was supplied by a grant from the Department of National Defense, Contract Number 2SU82-00334.

Finally, my special thanks are given to my parents for their patience and enormous support throughout my study at the University of Alberta. Thanks EAC.



## Table of Contents

<u>Chapter</u>	<u>Page</u>
1. Introduction .....	1
2. Description of Model .....	4
3. Outline of Solution .....	6
3.1 Formation of Flow Field .....	6
3.2 Calculation of Droplet Trajectory .....	9
3.3 Mechanisms of Heat Transfer .....	13
4. Results and Discussion. ....	19
4.1 Dynamic and Thermodynamic Equilibrium of the Droplet .....	20
4.2 Gravitation and Focusing Effect .....	31
4.3 Prediction of Liquid Water Content .....	36
4.4 Comparison of Wind Tunnel Characteristics (Batchelor & Shaw Versus Cubic Equation Type) .....	42
4.5 Comparison of Focusing Effect .....	48
4.6 Prediction Comparison Between 1-D Program and Axi-symmetric Program .....	51
5. Conclusions and Recommendations .....	53
REFERENCES .....	56
APPENDIX A: Flow Field Calculation Details .....	57
B: Listing of Programs .....	72
FLOW (Flow Field Computation) .....	73
MAIN (Trajectory and Temperature Calculation) .....	77
LIESUB (Program Subroutines) .....	87

## List of Figures

<u>Figure</u>	<u>Page</u>
3.1 Notation and measuring system of an axi-symmetric body .....	7
3.2 FROST tunnel set-up for computer program .....	11
4.1 The effect on thermodynamic equilibrium of the droplet due to droplet size and test section velocity for the FROST tunnel .....	21
4.2 The effect on dynamic equilibrium of the droplet due to droplet size and test section velocity for the FROST tunnel .....	22
4.3 Comparison of air and droplet velocities along the FROST tunnel for 50 micron droplets .....	26
4.4 Comparison of air and droplet velocities along the FROST tunnel for 100 micron droplets .....	27
4.5 Comparison of air and droplet temperatures along the FROST tunnel for 50 micron droplets .....	29
4.6 Comparison of air and droplet temperatures along the FROST tunnel for 100 micron droplets .....	30
4.7 Prediction of gravitational and focusing effect of the FROST tunnel on 100 micron droplets at a test section speed of 10m/s .....	32
4.8 Trajectories of 100 micron droplets inside the FROST tunnel at a test section speed of 10m/s ..	33
4.9 Prediction of gravitational and focusing effect of the FROST tunnel on 100 micron droplets at a test section speed of 25m/s .....	35
4.10 Prediction of gravitational and focusing effect of the FROST tunnel on 100 micron droplets at a test section speed of 50m/s .....	36
4.11 LWC profile at the centre of the test section of the FROST tunnel at a test section speed of 10m/s .....	38
4.12 LWC profile at the centre of the test section of the FROST tunnel at a test section speed of 25m/s .....	39

<u>Figure</u>	<u>Page</u>
4.13 LWC profile at the centre of the test section of the FROST tunnel at a test section speed of 50 m/s .....	40
4.14 Grid system for LWC prediction .....	41
4.15 Profile of Batchelor & Shaw type and Cubic Equation type contraction .....	43
4.16 Comparison of thermodynamic equilibrium .....	45
4.17 Comparison of dynamic equilibrium .....	47
4.18 Comparison of focusing effect at a test section speed of 10 m/s .....	49
4.19 Comparison of focusing effect at a test section speed of 25 m/s .....	50
A.1 Notation and measuring system of an axi-symmetric body .....	59
A.2 Analysis of velocity potential due to a circular ring source .....	63
A.3 Analysis of velocity potential due to a singular subelement .....	66

## Nomenclature

### Symbol

A	-projected area of the droplet, $m^2$
Cd	-coefficient of drag
Df	-diffusivity of water vapour in air, $m^2/s$
Fdrag	-aerodynamic drag force, N
h	-heat transfer coefficient, $J/m^2 \cdot C$
h <sub>d</sub>	-mass heat transfer coefficient, $kg/s \cdot m^2 \cdot K$
k	-thermal conductivity of air, $J/m \cdot K$
L	-distance between two points, m
Lv	-latent heat of vaporization, J/kg
$\nu$	-kinematic viscosity, $m^2/s$
Nu	-Nusselt Number
P	-vapour pressure, $N/m^2$ (Pa)
Pr	-Prandtl Number
$\dot{Q}$	-heat transfer rate, J/s
$\dot{Q}_0$	-heat transfer rate of stationary water droplet, J/s
r	-radius of water droplet, m
Re	-Reynolds Number
Rv	-universal gas constant, $J/kg \cdot K$
Sc	-Schmidt Number
Sh	-Sherwood Number
T	-temperature, K
t	-time, s
U <sub>a,d</sub>	-velocity of air and water droplet respectively, m/s
$\psi(p)$	-velocity potential at a point 'p', $m^2/s$

Symbol

- $\sigma(q)$  -surface source density at a point 'q'
- $\sigma'$  -Stefan-Boltzmann Constant,  $J/m^2 \cdot s \cdot K^4$
- $\iint_S ds$  -surface integral
- $\rho_{a,d}$  -density of air and water droplet respectively,  
 $kg/m^3$

## Chapter One

### Introduction

In recent years, ice accumulation on objects such as power lines, aircraft wings, helicopter blades and ships have caused concerns to people in different areas of society. For example, people in meteorology who want to predict the occurrence of freezing rain and send out warnings, people in aviation who want to find out the severity of freezing rain attacks which force the closure of airports, or researchers who want to find out the causes and effects of ice accumulation on objects such as airfoils, powerlines, etc. All they are hoping to do is to predict, anticipate, send out warnings or invent devices to minimize the damages caused by these naturally occurring events.

Results of these incidents can be devastating, for instance, the catastrophic accident of the Air Florida Boeing 737 in January 1982 at Washington D.C. near National Airport which killed 78 people. The frequency of helicopter loss in north eastern Canada in snow storms prompted the establishment of legislation to restrict helicopter flying under bad weather conditions during the winter. The safety of sea transportation is also endangered by cold weather conditions. Sea spray freezes and accumulates on the vessel superstructure causing stability problems. Land

transportation can also be crippled by bad weather. Therefore all types of transportation are affected by severe weather conditions in one way or another. Cities near coastal areas in the northern hemisphere are particularly susceptible to accidents that are icing related, primarily because the climate provides conditions favourable for ice accretion. Specific areas such as Northern Quebec are very susceptible to aviation problems and coastal areas in European countries such as Finland and Norway are more susceptible to capsizing of vessels and collapsing of power lines.

Researchers in the field of ice accumulation have been trying to examine the ice accretion process by attempting to simulate some of the conditions of icing in wind tunnels. These experiments are aimed at gaining insight into the problems and to develop some physical models of the icing process. Physical models that can be used to predict the amount of ice accumulation on an object, type of ice that forms under different types of weather conditions, shapes of ice formations on different surfaces, etc. All this information would lead to more accurate predictions of ice accumulation on objects. With this information, some devices may eventually be invented to minimize or prevent ice accumulation on critical parts of vessels or aircraft.

Wind tunnel testing, combined with computer modeling, is now being undertaken to analyse and predict the ice

accumulation on objects. In some of these computer models the velocity and temperature of the droplets prior to impact are required as input data. At present, there is no direct method which can measure the temperature of droplets and it is very difficult to measure the velocity of the droplet. These two droplet properties are usually assumed to be the free stream air values. The accuracy of this assumption and the effect of this assumption on the model predictions are not known. In this study, an attempt to estimate these two properties was undertaken for flow in a wind tunnel using a computer model.

The estimation of the properties of water spray is also of interest to meteorologists. Heather E. Auld (1980), Department of Meteorology at University of Alberta, developed a 'one-dimensional' model for predicting the temperature and velocity of water droplets which undergo dynamic and thermodynamic changes inside wind tunnels. The scope of this thesis extends the work of Auld by developing a general algorithm which predicts the two aforementioned droplet properties for any wind tunnel with an axi-symmetric cross section. Two major differences that appear in the more general model are the effects of gravity and a "focusing effect" produced by the droplet inertia on the droplet trajectory. Focusing effect is caused by the radial component of the momentum of the droplet after it passes through the contraction. It has a tendency to move the droplet toward the centre of the tunnel. —



## Chapter Two

### Description of the Model

The estimation of the dynamic and thermodynamic properties of droplets inside the wind tunnel is divided into three parts. First, the flow field inside the wind tunnel is established. The trajectory of the droplet are then calculated, and lastly, the heat exchange between the droplet and the free stream is computed.

In order to estimate the properties of the droplet correctly, it is important to establish a flow field that is similar to the actual one inside the wind tunnel. The droplet trajectory depends on the flow field which propels the droplet along the wind tunnel. The heat transfer is dependent on the duration of the trajectory of the droplet. In this study, the exact solution of the Neumann problem (A.M.O. Smith 1958) for arbitrary boundaries was used. This is a well established method for calculating flow over bodies of arbitrary shape. The bodies can have either two-dimensional or axi-symmetric cross sections. In this study we concentrated on the axi-symmetric case. The flow field was assumed to be an incompressible potential flow. In general, the bulk of the flow pattern inside the wind tunnel, especially at the centre of the tunnel, is a potential flow.

The motion of the droplet is described by Newton's

Second Law of Motion. Droplets are assumed to be rigid spheres. The drag force, propelling the droplet along the tunnel, was obtained from the relative velocity between the free stream and the droplet. By using a numerical integration technique, both velocity and position of the droplet were calculated.

The temperature change of the droplet was obtained by calculating the rate of heat exchange with the flow field. The heat transfer terms considered were evaporative, convection, radiation and the internal energy of the droplet.

Details of the general theories are described in Chapter Three. Chapter Four shows some of the results deduced from the computer program and the discussion of the results. A copy of the complete FORTRAN computer programs and subroutines are listed in Appendix B.

## Chapter Three

### Outline of the Solution

#### 3.1 Formation of the Flow Field

Calculation of the flow field inside the wind tunnel was based on Neumann's method for calculation of the potential flow about or within arbitrary boundaries. A general description of this method is given in this section. Details of the theory are explained in full in Appendix A.

To be able to use Neumann's method, the wind tunnel was divided into a number of ring sources as illustrated in Figure 3.1. The length of each ring does not necessarily have to be the same. These rings were obtained by the rotation of a small segment of the wind tunnel about the central axis. The contour of the wind tunnel was described by a continuous curve in the vertical plane in X and Y co-ordinates. Each ring, either a source or sink, has a constant value of source density on the entire ring; therefore, there is a set of source densities on the entire surface. The values of the set of source densities are originally unknown and are determined by using the boundary condition of the surface of the wind tunnel. For solid non-permeable surface, the boundary condition is that the velocity component normal to the surface at the mid-point of each ring is zero.

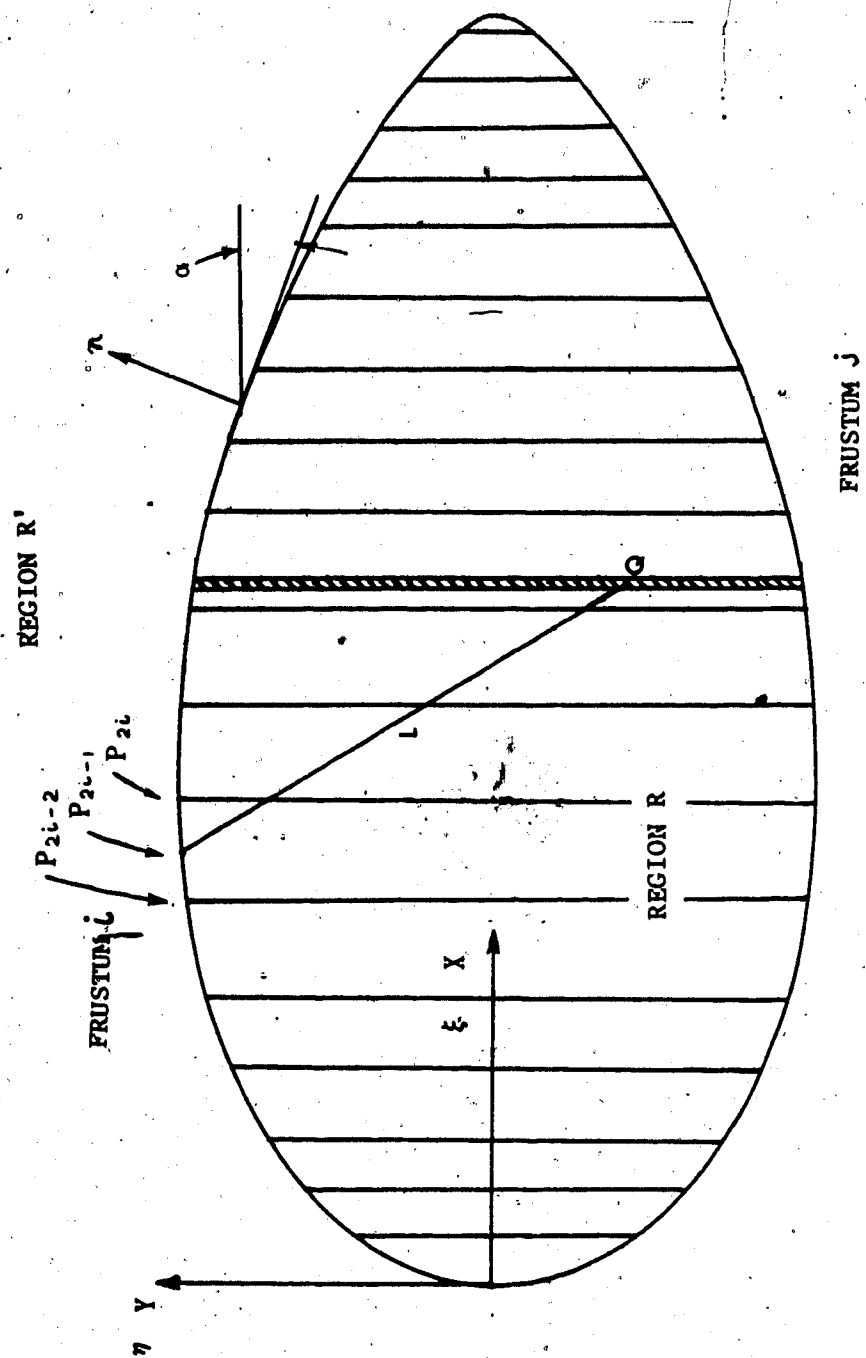


Figure 3.1 Notation and measuring system of an axi-symmetric body..

Figure 3.1 shows the notation and measuring system.  $P'$  represents an unbounded exterior region and  $P$  represents the interior region. The velocity potential at point  $P$  due to the influence of the whole body shell is:

$$\psi(P) = \iint_S \frac{\sigma(q)ds}{L} \quad (3.1)$$

In this Equation 3.1, the potential ( $\psi$ ) of point ' $P$ ' is calculated by the surface integral of the entire shell. The value ' $\sigma$ ' is the source density on the shell. Variable ' $L$ ' is the distance between ' $P_{2i-1}$ ' and the variable point ' $Q$ ' on the shell. This equation is valid for both regions  $P$  and  $P'$ . The velocity in any direction is then the derivative of the potential in that direction.

Integrating Equation 3.1 directly is quite complicated therefore a numerical method for integration was used. One of the simple and straight forward methods, Simpson's Rule, was employed here. It required that each ring be further divided into an even number of subelements. The number of subelements is inversely proportional to the distance between the ring and point ' $P$ '. The unknown value of the source density of each ring was solved by Equation 3.1 also. The boundary condition of each ring was specified at the midpoint of the ring. Since each of these points is influenced by all the other rings including itself, it can be easily seen that a set of  $n$  simultaneous equations is formed, where  $n$  is the total number of rings on the

object surface. This set of equations was then solved algebraically. Once the values of this set of source densities were evaluated, the potential and its derivatives (the velocities) at any point were readily obtained.

For the case of obtaining the source density of a wind tunnel, a special procedure was needed. The contour of the wind tunnel was described by a continuous curve starting from the centre of the centre of the wind tunnel. As this curve rotated about the central axis, a series of concentric rings were formed at one end of the wind tunnel (see figure 3.2). These vertical rings were acting as pumps to introduce flow inside the wind tunnel. This was done by specifying some values of velocity at the mid-point of each vertical ring, while the value of the velocity for the rest of the rings was specified as zero. The value of the velocity for these vertical rings was the same so that a uniform velocity profile at the test-section could be obtained. Uniform velocity profiles were obtained at locations -7.0 and -3.25 m of the FROST tunnel.

### 3.2 Calculation of the Droplet Trajectory

The motion of a single droplet in the air is governed by Newton's Second Law of Motion. The two major forces acting on the droplet are the viscous drag and the gravitational force. The equations of motion for a droplet have been derived and discussed in Auld's thesis (1980).

The equations have been simplified here to:

$$\vec{F}_{drag} = C_d * A * \rho_a * (\vec{U}_a - \vec{U}_d) \cdot (\vec{U}_a - \vec{U}_d / 2) * (\vec{U}_a - \vec{U}_d) / |\vec{U}_a - \vec{U}_d| \quad (3.2)$$

Justification for these simplifications have been discussed in Myron Oleskiw's thesis (1982).

In Equation 3.2 'Cd' is the coefficient of drag,  $\rho_a$  is the density of air and 'A' is projected area of the droplet and U is the velocity. Subscript 'a' denotes the properties of ambient air and 'd' denotes the droplet properties. The drag force is proportional to the square of the relative velocity ' $\vec{U}_a - \vec{U}_d$ ' between the free stream and the droplet. Bars over 'F' and 'U' indicate a vector quantity. The multiplication of the vector is done by dot product of the quantity. The vector direction for these variables are in the X, Y, and Z directions. By including the gravitational force acting on the droplet, all the forces on the droplet are accounted for. The forces acting on the droplet are expressed in the following equation

$$\vec{F} = \vec{F}_{drag} - (4/3\pi r^3) * \rho_d \vec{g} \quad (3.3)$$

All the values on the right hand side of Equation 3.3 are readily obtained either by the initial conditions or from the results of the previous time step. One exception is the value of 'Cd' (coefficient of drag). This value is calculated from a set of empirical formulae developed by Beard and Pruppacher (1969). They experimentally measured the drag force acting on water droplets falling at terminal velocity in air. The experimental correlations are valid for Reynolds Number ranging from 0.2 to 200. Later LeClair,

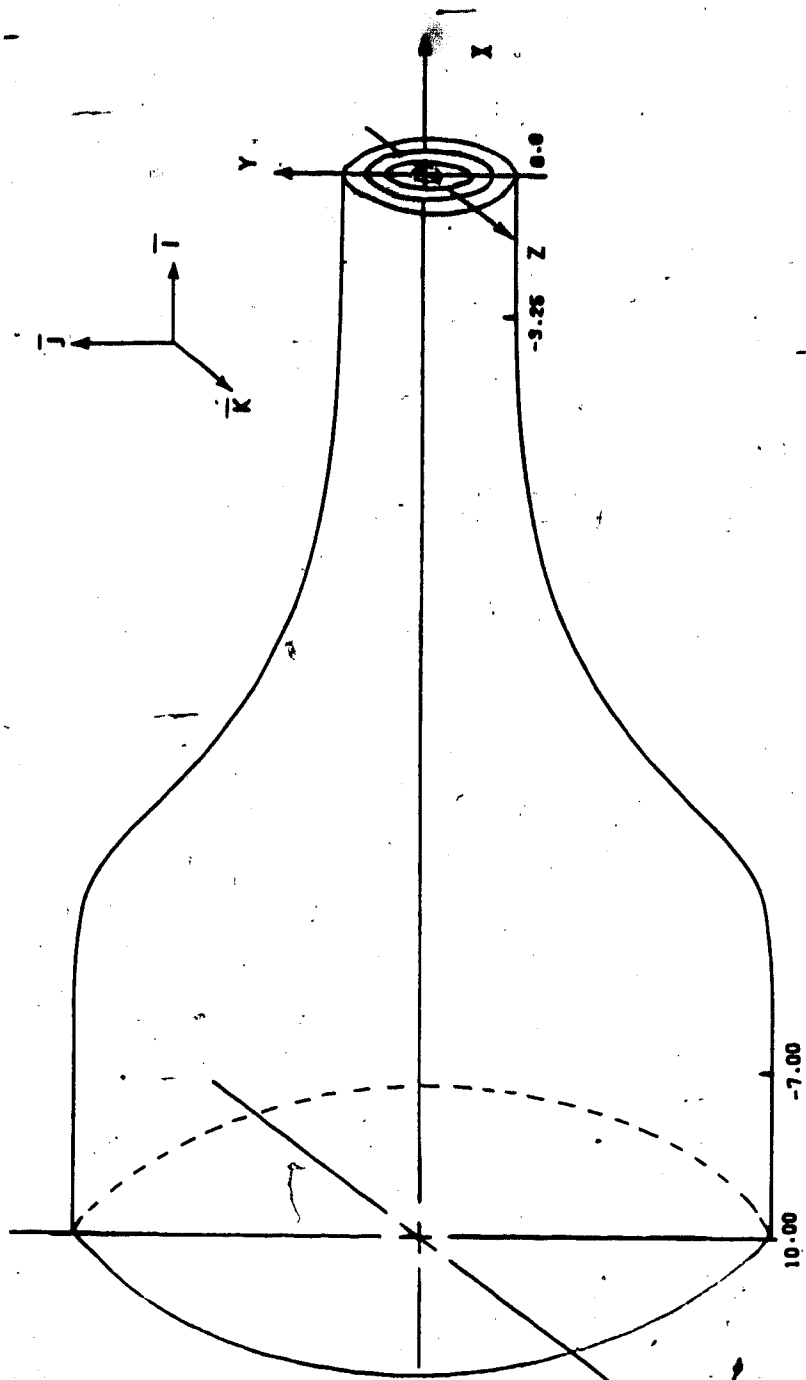


Figure 3.2 FROST tunnel set-up for the computer program.



et.al. (1970), theoretically predicted the values of viscous drag for rigid spheres for a Reynolds number range from 0.01 to 400. Their results agree with Beard and Pruppacher's experimental results. This agreement supports the simplification of treating water droplets as rigid spheres. The empirical drag coefficient described by Beard and Pruppacher is as follows:

$$C_d/(24Re) = 1 + A * Re^B \quad (3.4)$$

where  $A=0.102$ ,  $B=0.995$  for  $0.2 = Re < 1.5$   
 $A=0.115$ ,  $B=0.302$  for  $1.5 = Re < 20.0$   
 $A=0.189$ ,  $B=0.632$  for  $20.0 = Re < 200.0$   
 and,  $Re$  is the Reynolds Number.

Once the drag force on the droplet is evaluated, the change in velocity and position of the droplet can then be calculated by integrating the equations of motion.

Numerical integration is used to obtain the change in velocity and position. This is the most common method for integrating the equation of motion.

$$\int dF * dt / m = dU \quad (3.5)$$

$$\int dU * dt = dX \quad (3.6)$$

Equation 3.5 assumes that the drag force and the mass of the droplet are constant within the time interval. By integrating the ratio between the drag force and the mass of the droplet, that is the acceleration, with respect to time, we obtained the change in velocity of the droplet. Then the velocity was integrated with respect to time and we obtained the change in position of the droplet (Equation

3.6). The time step was obtained by a specified change in velocity of the droplet. A comparison was made between the results obtained by this method and Runge-kutta method and little different was found.

### 3.3 Mechanisms of Heat Transfer

To estimate the amount of heat transfer between the droplet and the free steam is a complicated and involved process. Difficulties such as circulation within the droplet, coalescence between droplets, and freeze-out of droplets make the problem difficult to solve. In order to calculate the amount of heat transfer, some assumptions have to be made. These are listed as follows:

1. The droplet is a rigid sphere with uniform temperature.
2. A single droplet is considered at one time, i.e. no droplet to droplet interaction.
3. Supercooling of the droplet is possible, therefore freeze out is not considered.
4. The thin layer of vapour surrounding the droplet is in equilibrium with the droplet, and the properties of this layer of gas are determined according to the temperature of the droplet.
5. Steady-state equations are used.
6. Density of air in the wind tunnel is constant.
7. Feed back on the air is not included; that is the air condition is not affected by the droplet.

Three types of heat exchange between the droplet and free stream were considered. They were evaporative heat transfer, convective heat transfer and radiative heat transfer. The net heat flux is equal to the change in internal energy of the droplet. The heat balance equation can be written as follows:

$$\dot{Q}_I = \dot{Q}_E + \dot{Q}_C + \dot{Q}_R \quad (3.7)$$

where subscript 'C' stands for convective, 'R' stands for radiative, 'E' stands for evaporative and 'I' stands for internal energy. All of these heat transfer components are rate of change of energy; that is, with respect to time.

The amount of evaporative heat transfer depends on the amount of water vapour transfer to or from the droplet surface. The rate of mass transfer is directly proportional to the difference in vapour density between the two mediums. According to Pruppacher and Klett (1978, p414), the rate of mass transfer of the droplet in steady state form is:

$$dM_c/dt = 4\pi r D_f (\rho_a - \rho_d) \quad (3.8)$$

where 'Df' is the diffusivity of water vapour in air and 'r' is the radius of the droplet. The subscripts have the same definitions as previously stated. Subscripts 'a' and 'd' refer to the properties of ambient air and water droplet surface respectively. The rate of latent heat exchange at the droplet surface is simply:

$$dQ_E/dt = 4\pi r D_f (\rho_a - \rho_d) * L_v \quad (3.9)$$

where 'Lv' is the specific latent heat of vaporization of water vapour. Assuming ideal gas behaviour for the vapour, the vapour density was substituted using the value of vapour pressure, temperature and the Universal gas constant (Rv). Equation 3.9 becomes:

$$dQ_E/dt = 4\pi r D_f L_v (P_a/T_a - P_d/T_d)/R_v \quad (3.10)$$

This substitution was made because temperature can be calculated easily and the vapour pressure is a function of temperature. The saturated water vapour pressure was obtained from an polynomial by P. R. Lowe (1976). The formulation is suitable for the temperature range from -50°C to 50°C. The expression, a sixth-order polynomial, has an error of less than one percent over this range.

The above expression applies to the latent heat transfer for stationary droplets only. When the droplets travel inside the wind tunnel, they are usually at a different velocity from the free stream. This relative motion enhances the heat transfer between the two mediums. In the field of heat transfer, this ventilation effect is accounted for by introducing a dimensionless number called Sherwood Number (Sh). This number is defined as:

$$Sh = h_d * (2r)/D_f \quad (3.11)$$

where 'h<sub>d</sub>' is the mass transfer coefficient, 'r' is the radius of the droplet and 'D<sub>f</sub>' is the diffusivity of water vapour.

The effect of the ventilation effect on the latent

heat transfer can be expressed as follows:

$$Q_E = (Q_E)_0 \cdot Sh/2 \quad (3.12)$$

where subscript '0' denotes heat transfer rate of stationary droplets. The value of the Sherwood Number is computed from the experiment results obtained by Beard and Pruppacher (1971). The empirical expression for the Sherwood number is as follows:

$$Sh/2 = 1.0 + 0.108(Sc^{1/3} Re^{1/2})^2 \quad Sc^{1/3} Re^{1/2} < 1.4$$

$$Sh/2 = 0.78 + 0.308(Sc^{1/3} Re^{1/2}) \quad 1.4 \leq Sc^{1/3} Re^{1/2} < 10$$

Sc is another dimensionless number called the Schmidt number. It is defined as the ratio between kinematic viscosity of air 'v' and diffusivity of water vapour 'Df'.

$$Sc = v/Df \quad (3.14)$$

A similar argument was used for the calculation of convective heat transfer. The ventilation effect was accounted for by introducing another dimensionless number, the Nusselt number (Nu), in a similar fashion as the Sherwood number for mass transfer. The Nusselt number is defined as:

$$Nu = h(2r)/k \quad (3.15)$$

where 'h' is the heat transfer coefficient, 'r' is the radius of the droplet and 'k' is the thermal conductivity of air. The heat transfer equation, according to Pruppacher and Klett (1978, p.418) is:

$$dQ_C/dt = 4\pi r k'' (T_a - T_d) Nu/2 \quad (3.16)$$

where k'' is the modified coefficient of heat transfer coefficient of moist air, which has units of J/cm<sup>2</sup>·sec·K

A similar expression for calculating the Sherwood number is used to calculate the Nusselt Number. It is computed by the following expressions:

$$Nu/2 = 1.0 + 0.108(Pr^{1/3}Re^{1/2})^2 \quad Pr^{1/3}Re^{1/2} < 1.4$$

$$Nu/2 = 0.78 + 0.308(Pr^{1/3}Re^{1/2}) \quad 1.4 \leq Pr^{1/3}Re^{1/2} < 16$$

Here Prandtl number 'Pr' was introduced replacing the Schmidt Number. The Nusselt number is therefore defined in terms of Prandtl number and Reynolds number. Prandtl number is defined as the ratio between kinematic viscosity 'v' and thermal conductivity of air 'k'.

$$Pr = v/k \quad (3.18)$$

The limit for the values of  $Sc^{1/3}Re^{1/2}$  and  $Pr^{1/3}Re^{1/2}$  is 16 which corresponds to flow with Re less than 320.

The final form of heat transfer is radiation. It was calculated according to Stefan-Boltzmann's Law. The expression for the heat transfer by long wave radiation is:

$$\dot{Q}_R = 4\pi r^2 \sigma E (T_a^4 - T_d^4) \quad (3.19)$$

where  $\sigma$  is the Stefan-Boltzmann constant which has a value of  $5.669 \times 10^{-8} \text{ J/m}^2 \cdot \text{sec} \cdot \text{K}^4$ . E is the emissivity of the droplet and is assumed to have a value of 1.0.

The sum of all three forms of heat transfer results in the change in internal energy of the droplet. The change in energy is written as:

$$\dot{Q}_I = 4/3 \pi r^3 \rho_d C_p (dT_d/dt) \quad (3.20)$$

where ' $\rho_d$ ' is the density of water and ' $C_p$ ' is the specific heat of water.

The energy balance equation for the droplet, according to Equation 3.7, can be written as follows:

$$\begin{aligned} \frac{4}{3}\pi r^3 \rho_d C_p \frac{dT_d}{dt} = & 4\pi r L_v D_f (P_a/T_a - P_d/T_d) (Sh/2)/Rv \\ & + 4\pi r k'' (T_a - T_d) Nu/2 \\ & + 4\pi r^2 \sigma' E (T_a^4 - T_d^4) \end{aligned} \quad (3.21)$$

The total change in energy is obtained by integrating the rate of heat transfer with respect to time. For convenience, the time step for integrating the equation of motion was used in this integration.

## Chapter Four

### Results and Discussion

This chapter presents and discusses some results obtained from this program. Most of the results in this chapter were obtained for the FROST icing wind tunnel of the Mechanical Engineering Department at the University of Alberta. Results represent the predictions of the dynamic and thermodynamic properties, final position of the droplet due to the gravity effect, and the focusing effect of the wind tunnel. The range of droplet sizes, from 10 microns to 100 microns, over a range of test section velocities from 10 m/s to 50 m/s were used as testing parameters. These ranges are identical to that used for actual experiments at the FROST wind tunnel. Also included is a comparison of the performance of two different types of wind tunnel contractions. This performance test illustrates the usefulness of the algorithm as a design tool.

To use the program, initial conditions for the droplet temperature, position and velocity were specified. Initial temperature of air and droplets were set at 263 K and 283 K respectively. The initial velocity of the droplets was usually close to that of the free stream at the specified location. From a study using the axi-symmetric program, it was found that the final results are not sensitive to the initial velocity of the droplet.



The FROST icing wind tunnel was designed by M. Sroka (1972) as a M.Sc. thesis. This tunnel was designed to have a minimal amount of turbulence (about 0.2 percent) at the test section. The tunnels octagonal cross section was represented by a inscribed circle and the contour is shown in Figure 3.2. The effect of this cross section on the results from this program, which predicts only axi-symmetric type wind tunnels, is minimal because most droplets are introduced far enough from the wall. Also the area ratio at any point with respect to the inlet is the same for both cross sections.

The initial position of the droplets was specified by X, Y, and Z co-ordinates. X is the direction along the axis of the wind tunnel. This co-ordinate indicates the location of the spray nozzles upstream from the centre of the test section. Using the Y and Z co-ordinates as shown in Figure 3.2, the location of a droplet across a vertical plane can be specified. In this way, the focusing and gravitational effect on the distribution of the liquid water content (LWC) were predicted by obtaining the final locations of the droplets at the test section.

#### 4.1 Dynamic and Thermodynamic Equilibrium of the Droplet

Figures 4.1 and 4.2 show the predictions of thermodynamic and dynamic equilibrium of the droplet at the centre of test section respectively. For these results, droplets were introduced into the free stream with only an axial velocity. An axial velocity, close to that of the free

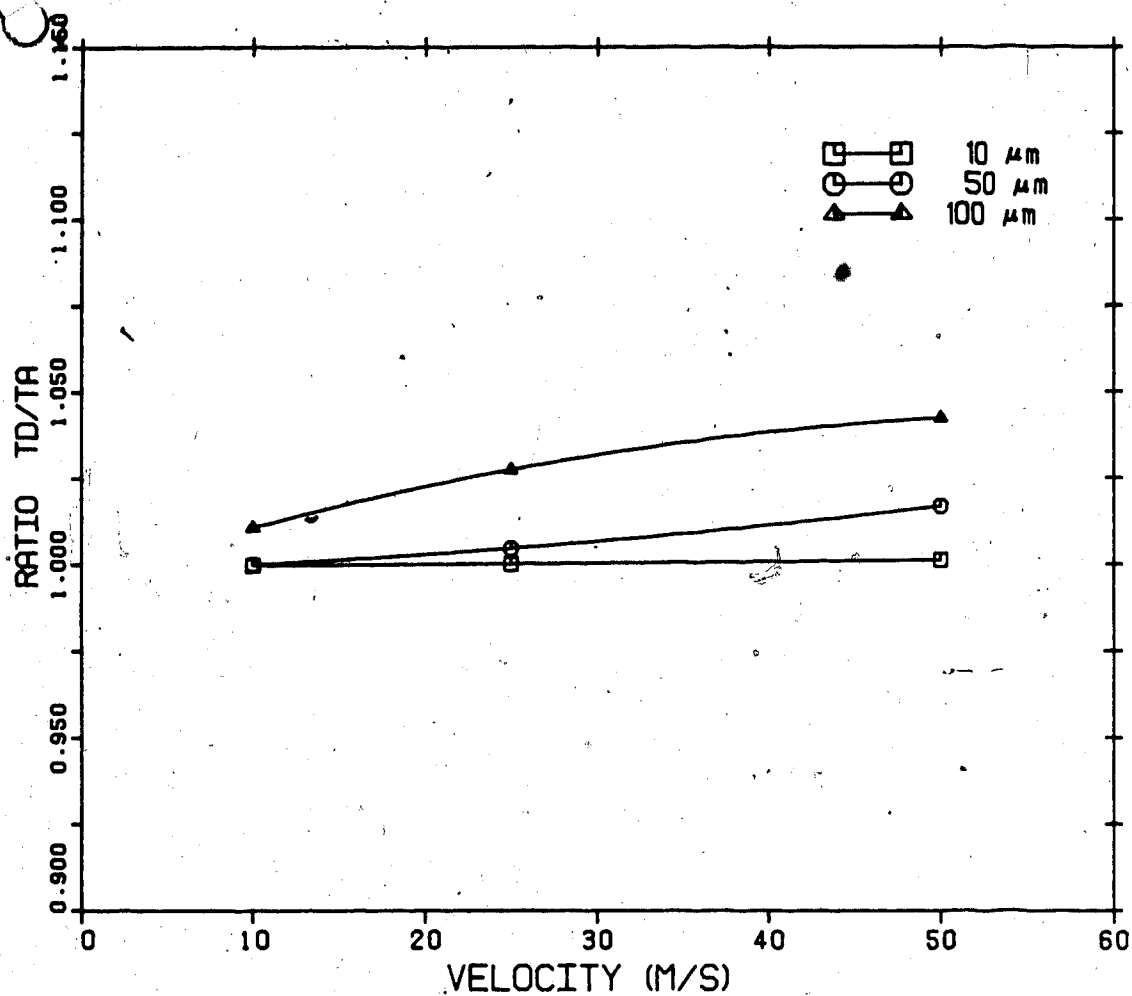


Figure 4.1 The effect on thermodynamic equilibrium of the droplet due to droplet size and test section speed for the FROST tunnel.

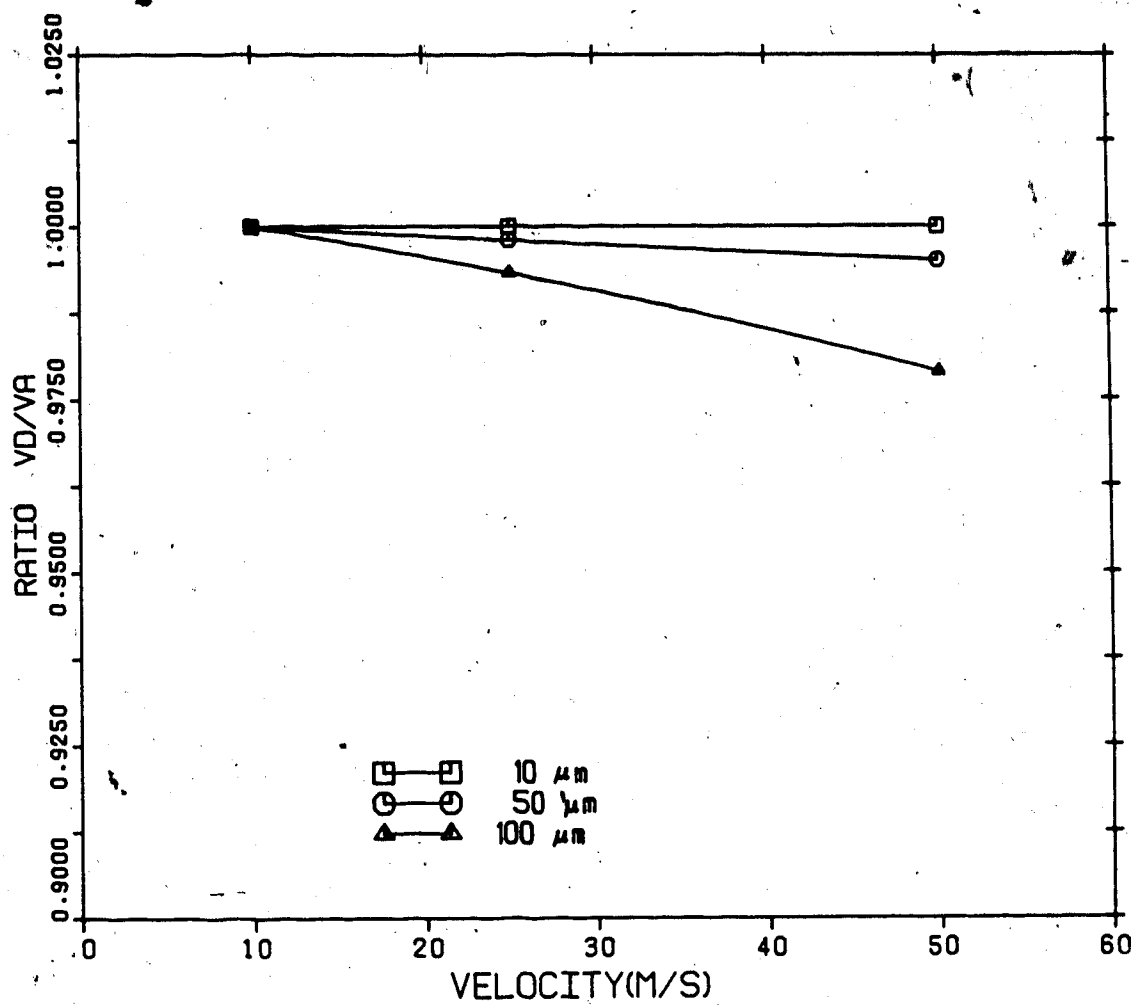


Figure 4.2 The effect on dynamic equilibrium on the droplet, due to droplet size and test section speed for the FROST tunnel.

stream, of 0.625m/s, 2.56m/s and 3.125 m/s was used at the initial position of 3 metres upstream from the centre of the test section. These velocities corresponded to test section velocities of 10m/s, 25m/s and 50 m/s respectively. The relative humidity of the air was specified as 50 percent. A decrease in relative humidity of the air decreases the final temperature of the droplet; therefore the droplet temperature decreases due to latent heat of vaporization. With the water spray turned on and the air circulating through the tunnel, it was difficult to measure the humidity of the air inside the tunnel; therefore, a mean value of 50 percent was used. The ordinate of these figures is the ratio of droplet temperature to air temperature and absolute temperature was used. The abscissa is the test section velocity in m/s.

The results show that 10 micron droplets achieved thermodynamic equilibrium with the free stream for all three test section speeds. However, for the bigger droplets (50 micron) thermodynamic equilibrium with free stream is only achieved with a test section speed of less than 10m/s.

From these results, it is obvious that the temperature deviation between the droplet and free stream can be explained by the total amount of heat transfer between the droplet and free stream. For higher free stream velocities, the droplets will spend less time inside the wind tunnel resulting in a smaller amount of heat transfer. Although the evaporative and convective heat transfer rates

increased, they are directly proportional to Reynolds number to a power of less than one; however, time is directly proportional to velocity which is directly proportional to the Reynolds number. The only exception is when the droplets reach equilibrium with the free stream before they reach the test section. In which case time will not affect the final temperature of the droplet.

The ambient temperature was assumed to be unaffected by the heat transfer with the droplet because only one droplet was considered at a time and ambient air was assumed to have a much larger mass. However, the ambient temperature did change when passing through the contraction. According to Energy equation, air undergoes adiabatic expansion as it rushes through the contraction. The law simply says air velocity increases and energy is expended causing a decrease in air temperature. For a test section speed of 50m/s at the FROST tunnel a temperature decrease of 2 K was predicted.

Dynamic equilibrium of the droplets with the free stream is shown in Figure 4.2. The vertical scale is the ratio of droplet velocity to the free stream velocity. The horizontal scale is the free stream velocity at the test section. For 10 micron droplets, the final velocity at the midpoint of the test section was almost identical to that of the free stream. For 50 micron and 100 micron droplets and at higher test section speeds, the final droplet velocity did not reach equilibrium with the free stream. This lagging in velocity could be due to the increase in body mass of the

droplet. The mass is proportional to the radius to the power of three while the drag force is proportional to the square of the radius. Therefore it is harder to accelerate a bigger droplet while it is relatively easy to accelerate a small droplet.

Figures 4.3, 4.4, 4.5 and 4.6 show the predictions of temperature and velocity of the droplets along the FROST icing wind tunnel. The exact contour of the tunnel is also shown in Figure 4.8. The location -3.25 metres on the x-axis is the midpoint of the test section. All droplets were introduced at a location of -7.0 metres on the x-axis. The initial conditions of the droplets were the same as stated before. The initial temperature of the droplet was at 283 K and the initial velocity was close to the free stream velocity

The three curves shown on each figure are results of three test section speeds of 10m/s, 25m/s and 50m/s. The curves that have no symbols are the properties of air. From the difference between the curves showing the properties of air and the droplet, we can find out at what locations the droplets are in equilibrium with the ambient air. This difference also indicates the effect of tunnel shape has on the equilibrium of the droplet.

Figures 4.3 and 4.5 show the temperature and velocity for 50 micron droplets respectively, while Figures 4.4 and 4.6 show similar results for 100 micron droplets. These figures provide additional information to the thermodynamic

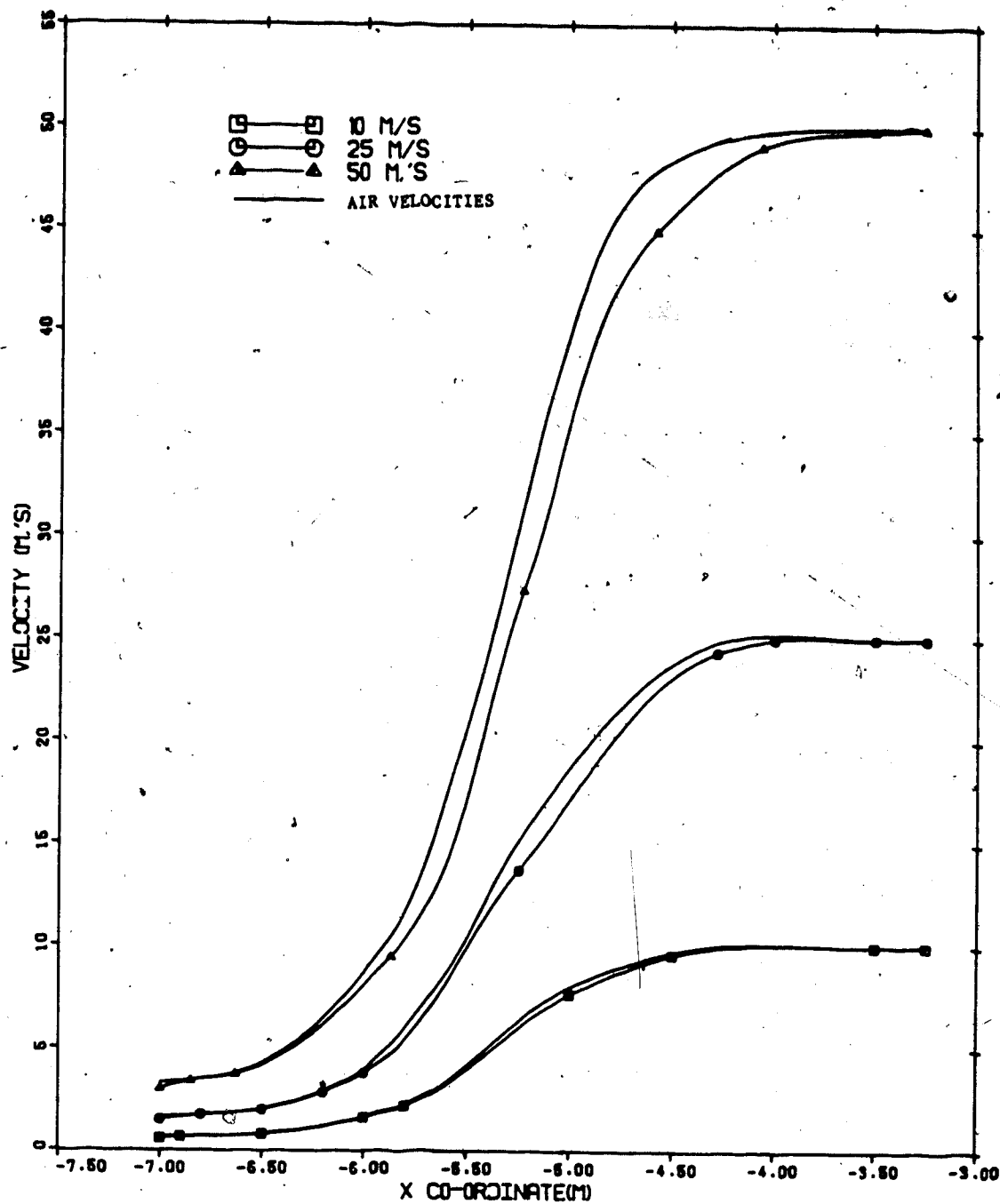


Figure 4.3 Comparison of air and droplet velocities along the FROST tunnel for 50 micron droplets.

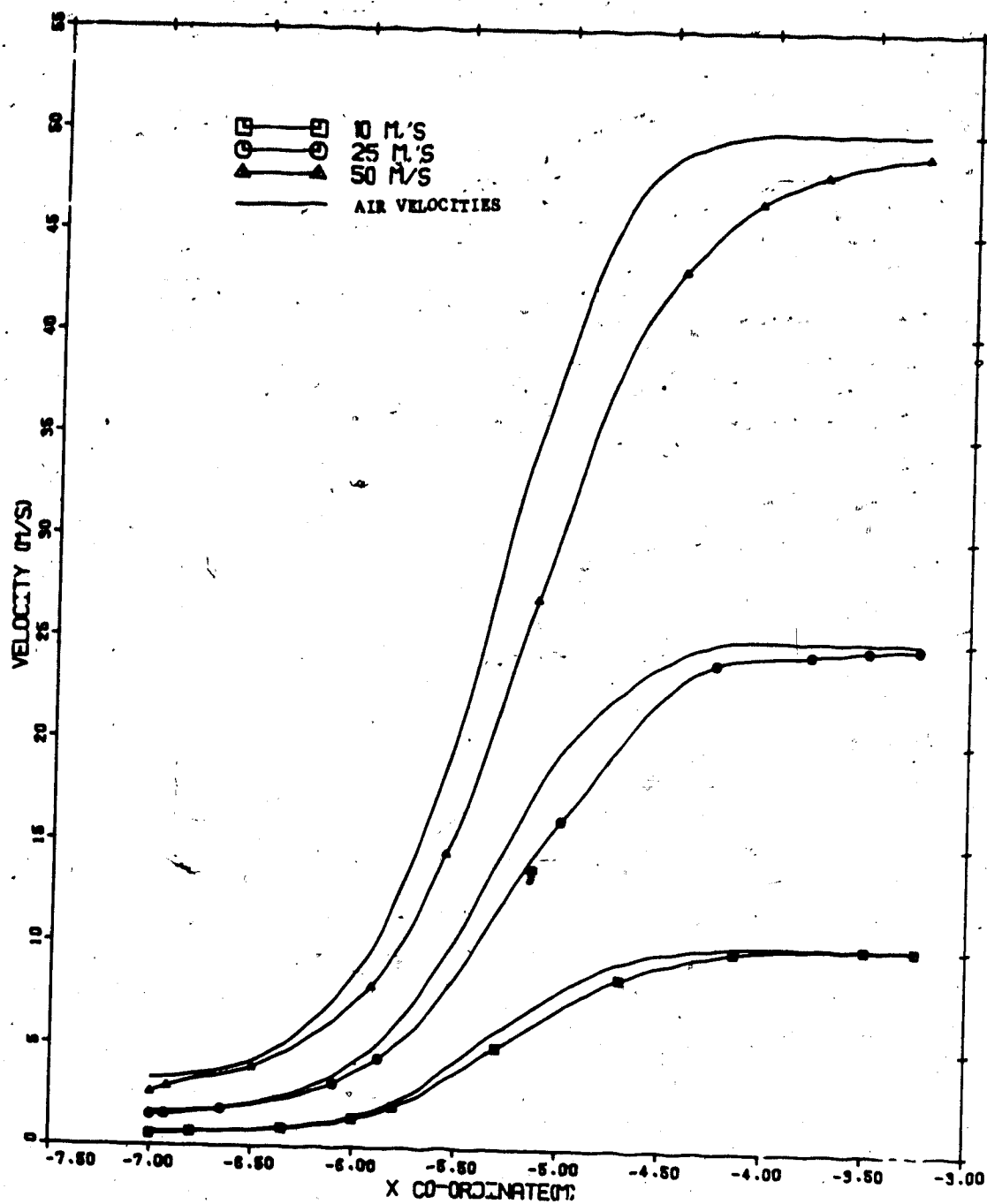


Figure 4.4 Comparison of air and droplet velocities along the FROST tunnel for 100 micron droplets.



and dynamic predictions in this section. Results for 10 micron droplets are not shown here because, from the trend shown by the 50 micron droplets, smaller droplets achieve equilibrium more easily than bigger droplets.

In Figures 4.5 and 4.6, the temperature of the droplet decreases rapidly at the beginning and slowly levels off as the droplet approaches the test section. For the 50 micron droplets, the droplets travelling at a higher tunnel speed have a lower final temperature. This can be explained by the fact that the air temperature at 50m/s cools down to a lower value due to the increase in air speed. Smaller droplets have smaller mass therefore they can catch up to the decrease in air temperature. Bigger droplets, such as 100 microns, the droplet temperature deviates from the air temperature very distinctively at all tunnel speeds.

Figures 4.3 and 4.4 show the velocity of the droplet along the icing tunnel. At the beginning of the tunnel, the droplets reach the air velocity very quickly for both sizes of droplets. As the air velocity increases through the contraction section, the droplet velocity begins to lag behind the air velocity; however, the final velocity of the smaller droplets still reach equilibrium with free stream at the test section. For bigger droplets, the droplet speed lags the air speed considerably especially at high tunnel speed.

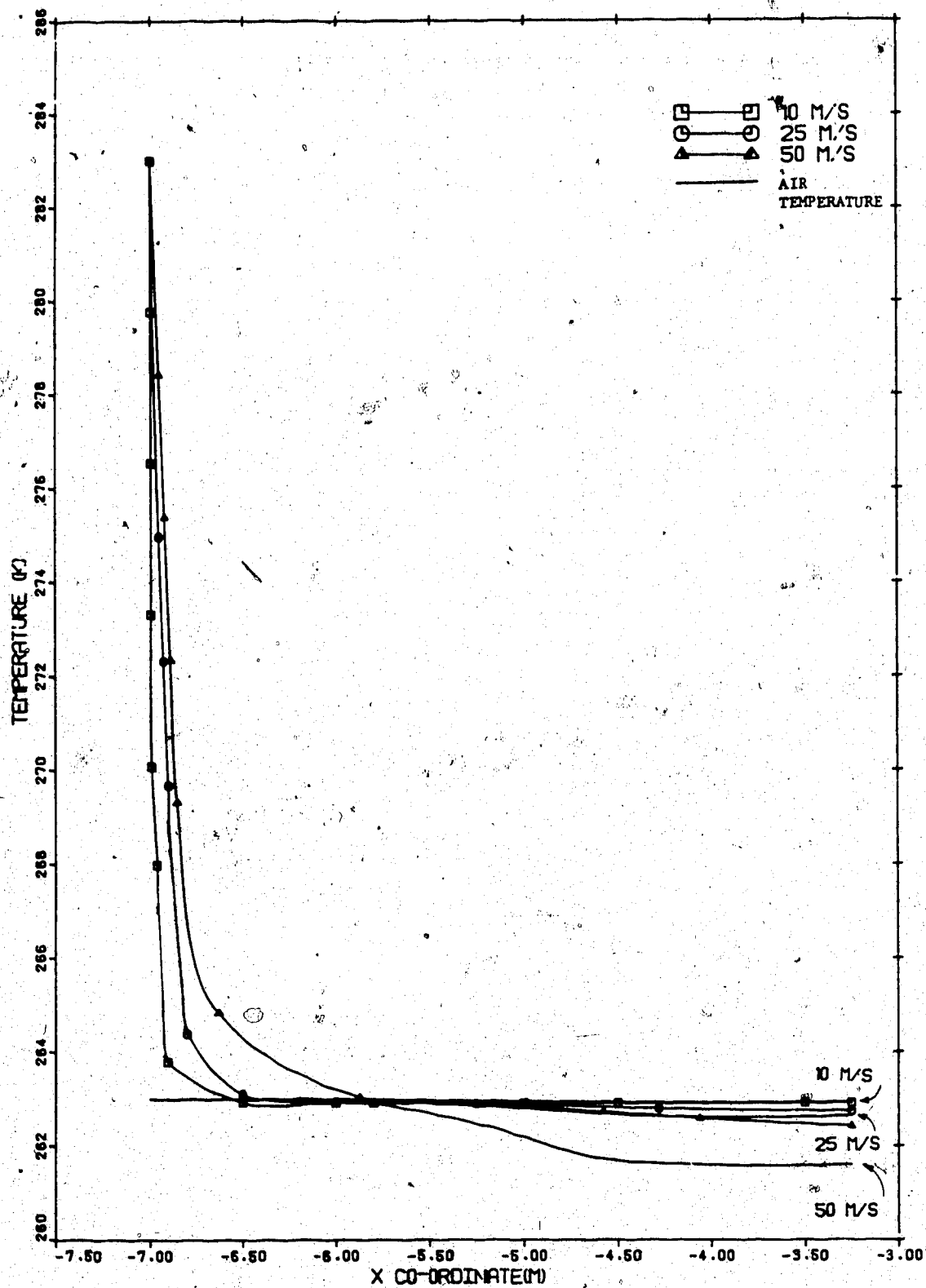


Figure 4.5 Comparison of air and droplet temperatures along the FROST tunnel for 50 micron droplets.

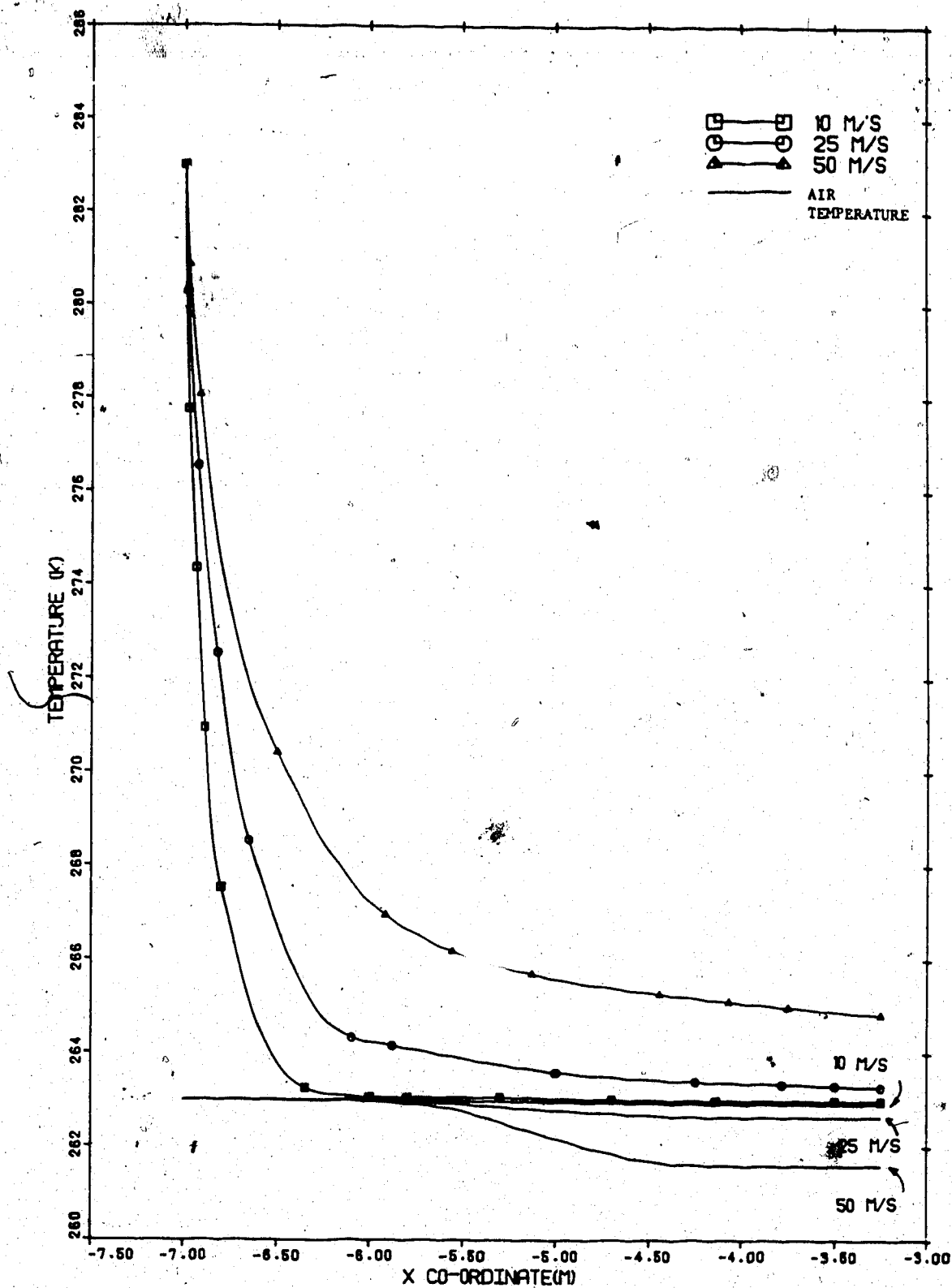


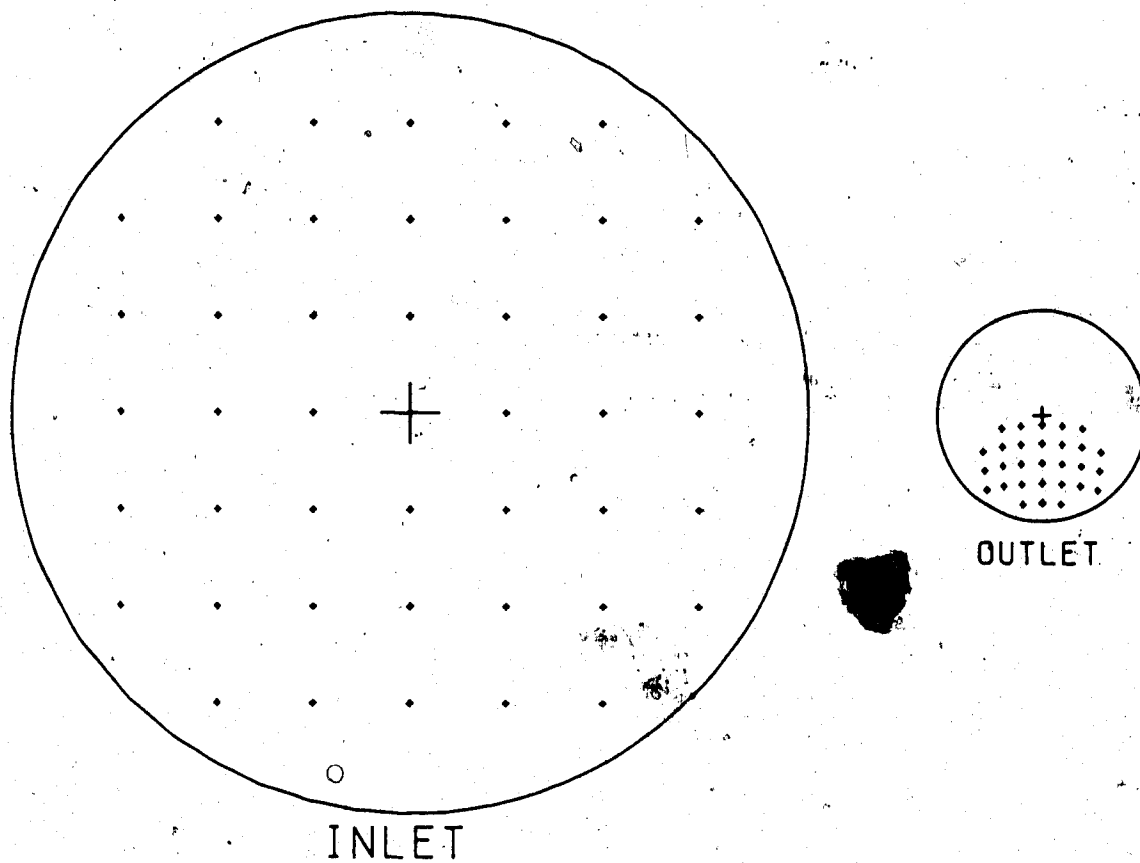
Figure 4.6 Comparison of air and droplet temperatures along the FROST tunnel for 100 micron droplets.

#### 4.2 Gravitational and Focusing Effect

The predictions of the gravitational and focusing effect of the wind tunnel are shown in Figures 4.7, 4.9 and 4.10. These figures are results for 100 micron droplets with test section velocities of 10m/s, 25m/s and 50 m/s respectively. The results were obtained by setting up a uniform grid of droplets at the inlet of the tunnel, as shown on the left hand side of these figures. From the final position of the droplets obtained from the program, a different droplet pattern at the outlet of the wind tunnel is formed. By studying and comparing the final grid configuration, the gravitational and focusing effects can be observed.

This program can only predict one trajectory at a time, therefore the final grid was formed by recording the final positions separately. Since the left and right half of the tunnel are mirror images of each other, trajectories for only half of the droplet were computed.

Figure 4.7 shows the results for a test section speed of 10m/s. The majority of the droplets end up at the lower section. Some droplets were lost when they collided with the lower part of the tunnel wall and never reached the test section. This can be seen more clearly in Figure 4.8 which shows the history of the total trajectories for some droplets. The figure shows the vertical centre plane only because it is free from the focusing effect due to the left and right half of the side walls, the effect of which can



DROPLET DIAMETER 0.0001M  
OUTLET AIR VELOCITY 10.0M/S  
CONTRACTION RATIO 16:1

Figure 4.7 Prediction of gravitational and focusing effect of the FROST tunnel on 100 micron droplets at test section speed of 10 m/s.

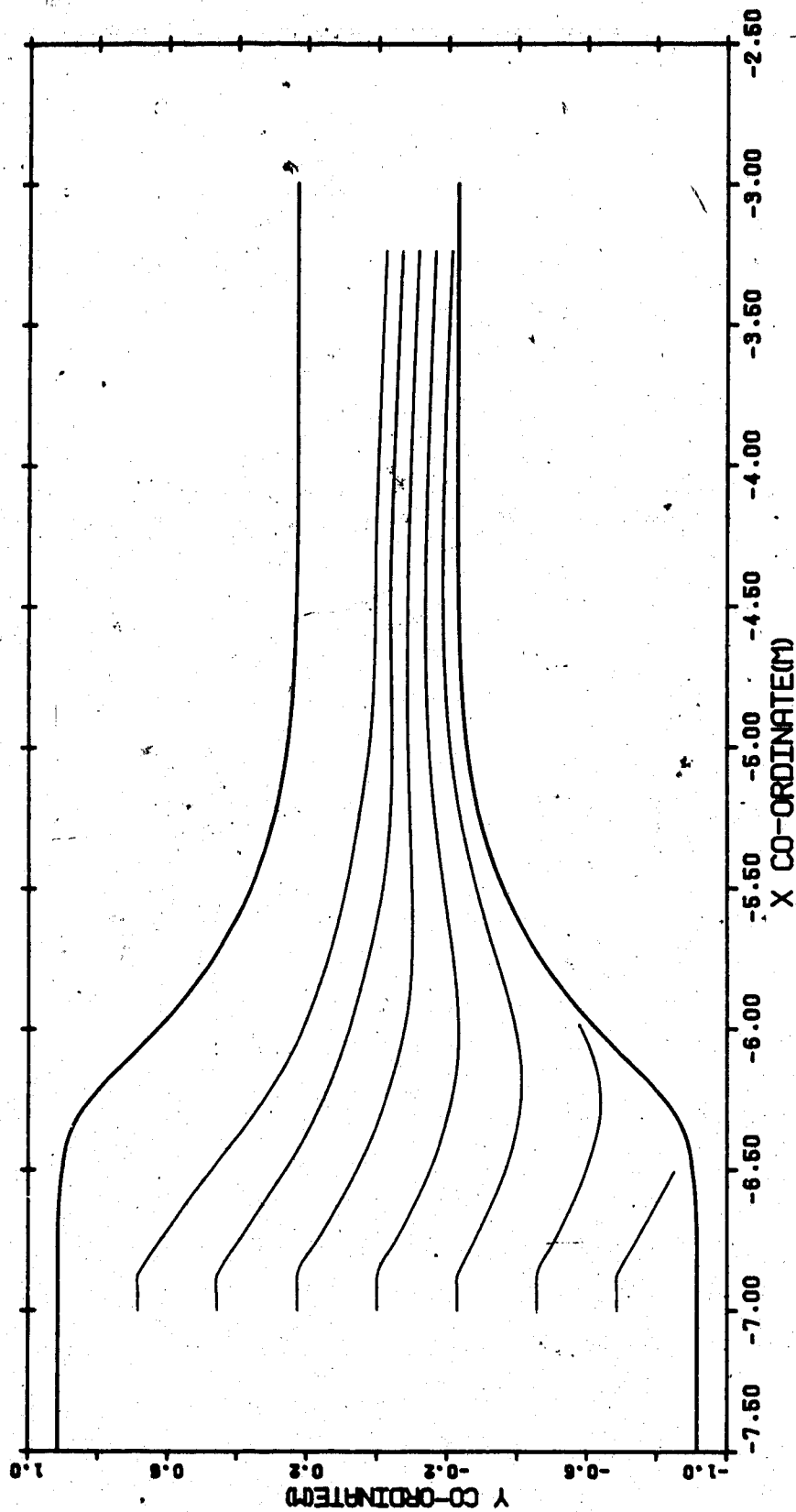


Figure 4.8 Trajectories of 100 micron droplets inside the FROST tunnel at a test section speed of 10 m/s.

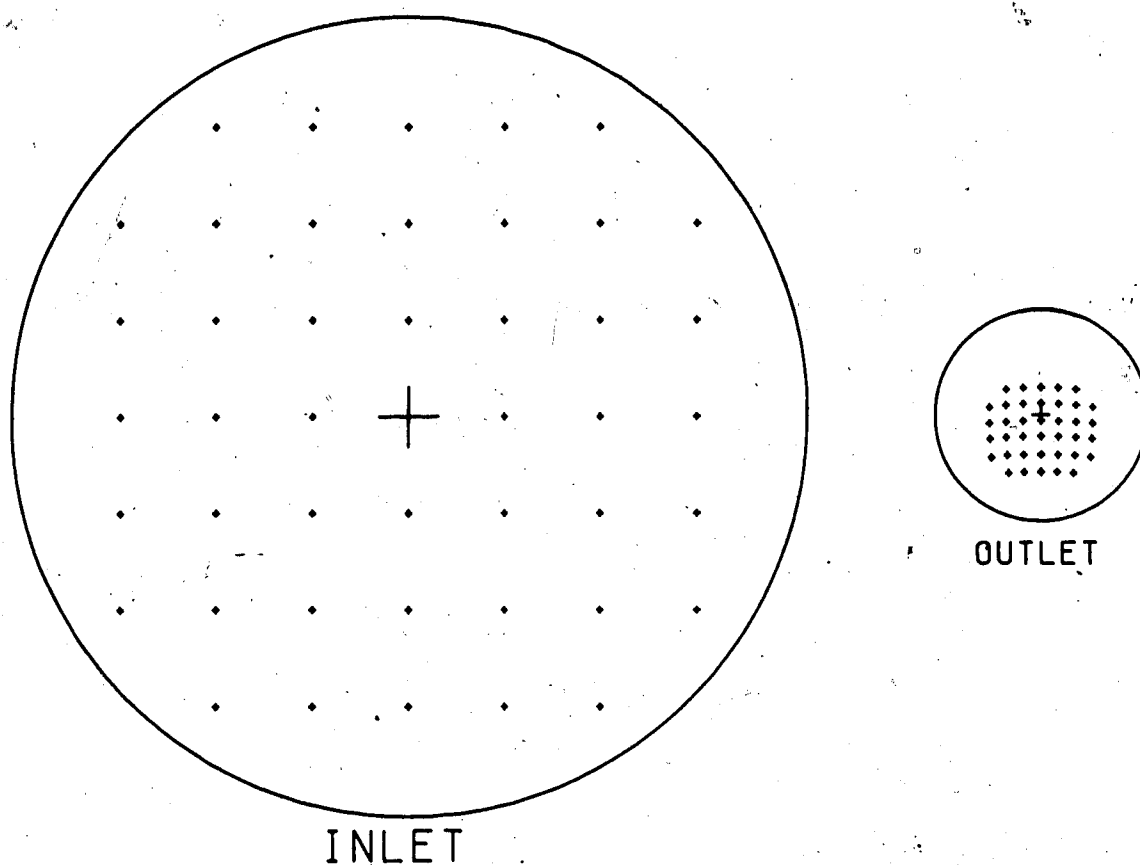
only be shown on a three dimensional figures. The gravitational and focusing effects can easily be seen here. It can be said that the gravitational effect is more dominant than the focusing effect in this case.

Figures 4.9 and 4.10 are the results for higher test section velocities. They show that the focusing effect is more dominant than the gravitational effect. Even though the final grid is lower than the original, there were no droplets disappearing due to collisions with the wall. The droplets group together at the centre section mainly due to the focusing effect. For higher velocities the cluster of droplets is tighter and a smaller grid is formed. The location of the entire group was also higher than a grid at a lower velocity. Hence it can be concluded that the focusing effect is more dominant at higher velocities.

Similar results can be obtained for smaller droplet sizes of 10 microns and 25 microns; however, the results are not shown here. It was also found that the gravitational effect does not affect smaller droplets as much. No droplets were lost due to collisions with the lower tunnel wall even at low test section velocities.

#### 4.3 Prediction of Liquid Water Content Across the Tunnel

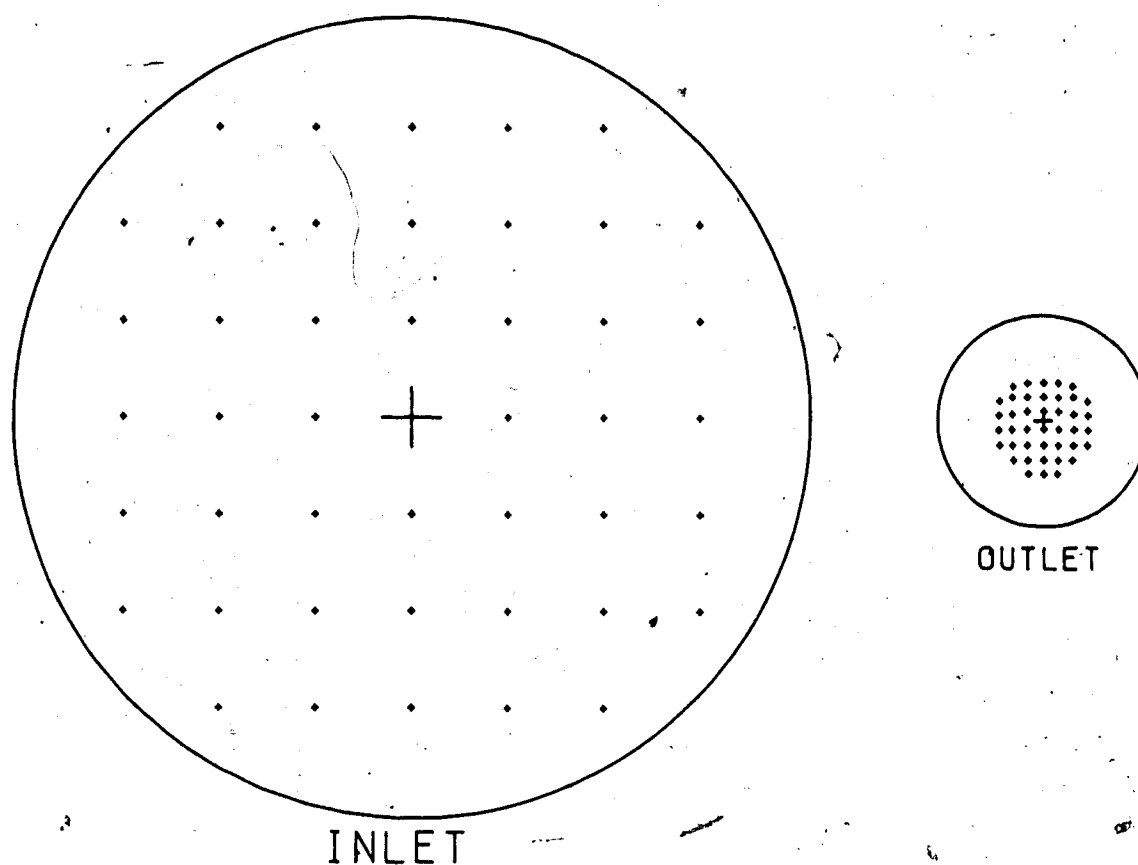
By using the results obtained from these three sizes of droplets, we can analyse the variation of the liquid water content (LWC) across the plane at the midpoint of the test section. LWC is defined as the amount of water across a



DROPLET DIAMETER 0.0001M  
OUTLET AIR VELOCITY 25.0M/S  
CONTRACTION RATIO 16:1

Figure 4.9 Prediction of gravitational and focusing effect of the FROST tunnel on 100 micron droplets at test section speed of 25 m/s.





DROPLET DIAMETER 0.0001M  
OUTLET AIR VELOCITY 50.0M/S  
CONTRACTION RATIO 16:1

Figure 4.10 Prediction of gravitational and focusing effect of the FROST tunnel on 100 micron droplets at test section speed of 50 m/s.

unit area per unit time. In Figures 4.11, 4.12, and 4.13 we show the predictions of the LWC at the mid-point of the test section for test section speeds of 10m/s, 25m/s and 50 m/s respectively. The results were obtained according to the following procedures. A uniform grid was set up upstream of the test section and a corresponding grid was also set up at the test section (see Figure 4.14). Each square consisted of some distribution of the three sizes of droplets. According to a study by E.M. Gates and E.P. Lozowski (1984), the dominant droplet size for the FROST tunnel is 30 microns. By varying the percentage of each of the three droplet sizes occupying at the squares, a volume medium droplet diameter of 30 microns was produced.

Droplets of 10 microns, 50 microns and 100 microns were introduced at the centre of each square. The final positions of the droplets predicted by the program were then recorded. The number of droplets of each size passing through each square were counted and the total amount of water was calculated accordingly. This value was plotted at the centre of each square. Using the maximum LWC as reference, only a relative value was plotted

The results obtained by this method are not in agreement with some experimental results. From most experimental results, especially for dry icing, maximum ice accumulation is at the centre line Y'-Y'' of the cross section (see Figure 4.14). The current study predicted a lowest value on this line. This discrepancy can be

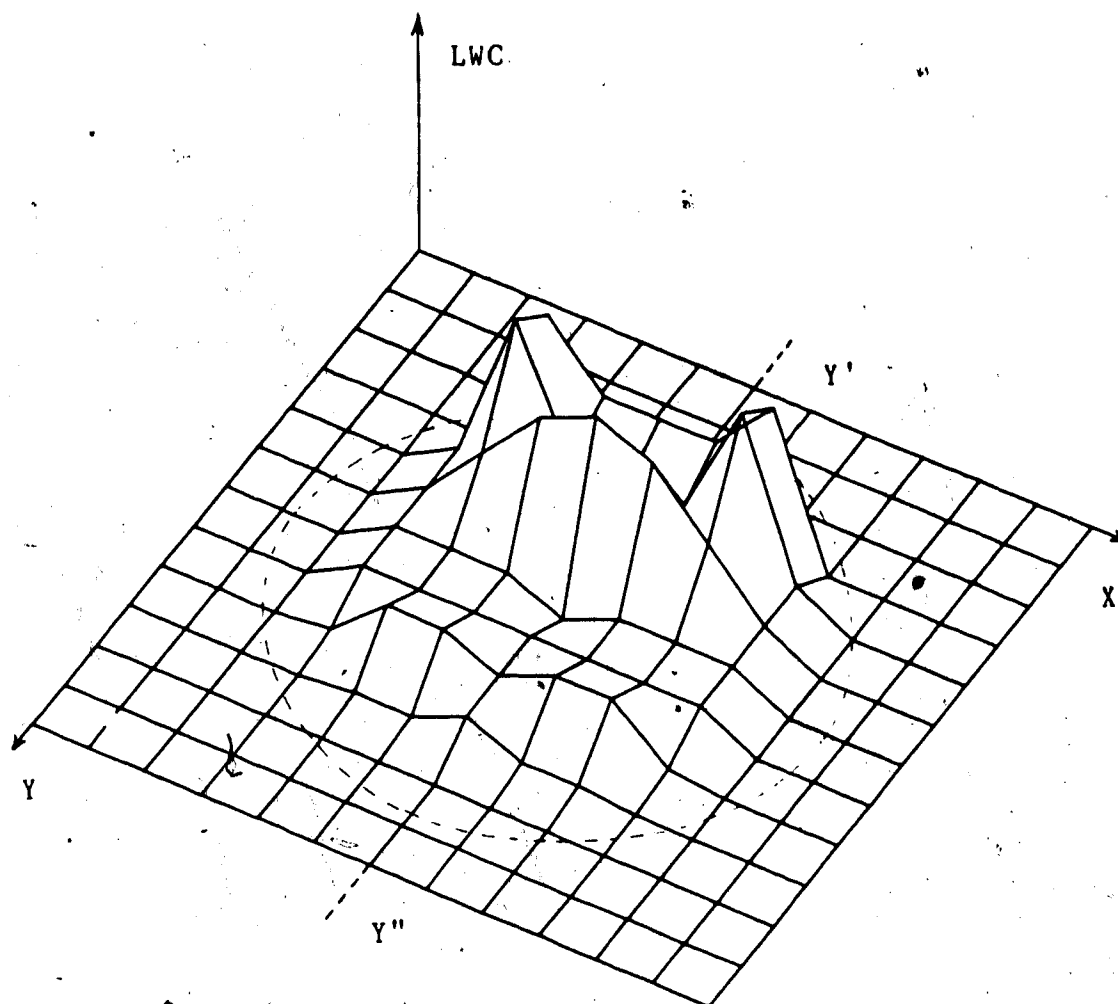


Figure 4.11 LWC profile at the centre of the test section of the FROST tunnel at a test section speed of 10 m/s.

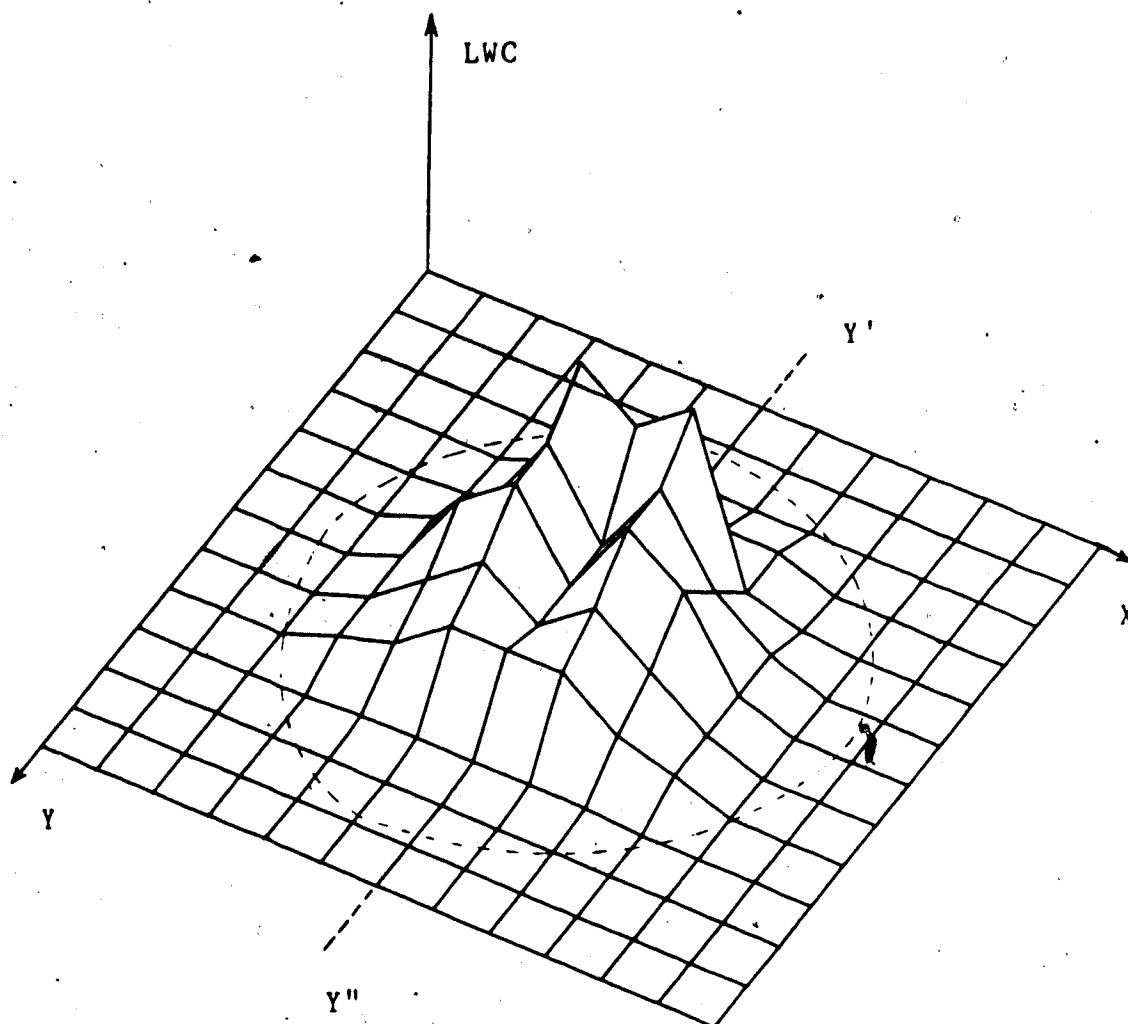


Figure 4.12 LWC profile at the centre of the test section of the FROST tunnel at a test section speed of 25 m/s.

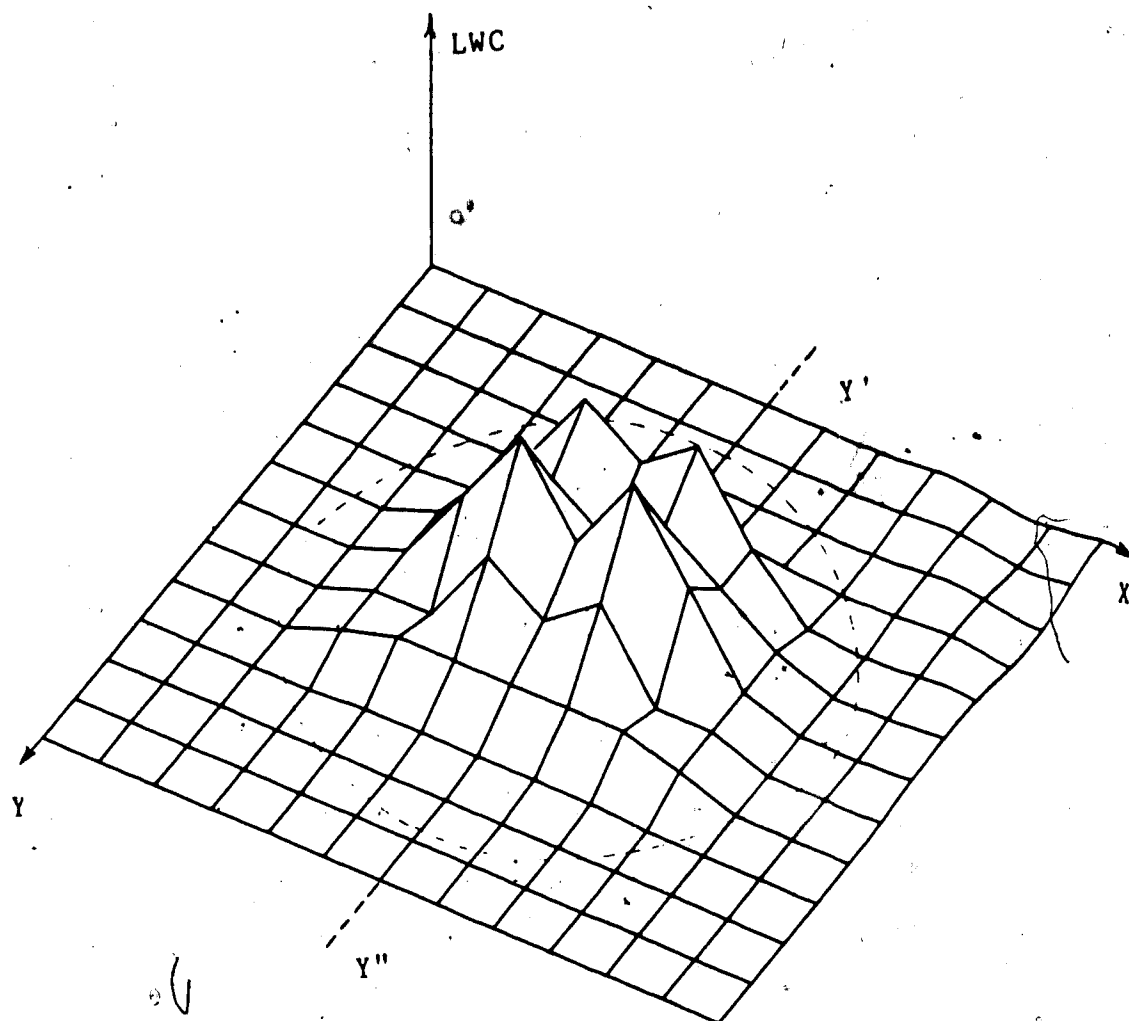


Figure 4.13 LWC profile at the centre of the test section of the FROST tunnel at a test section speed of 50 m/s.

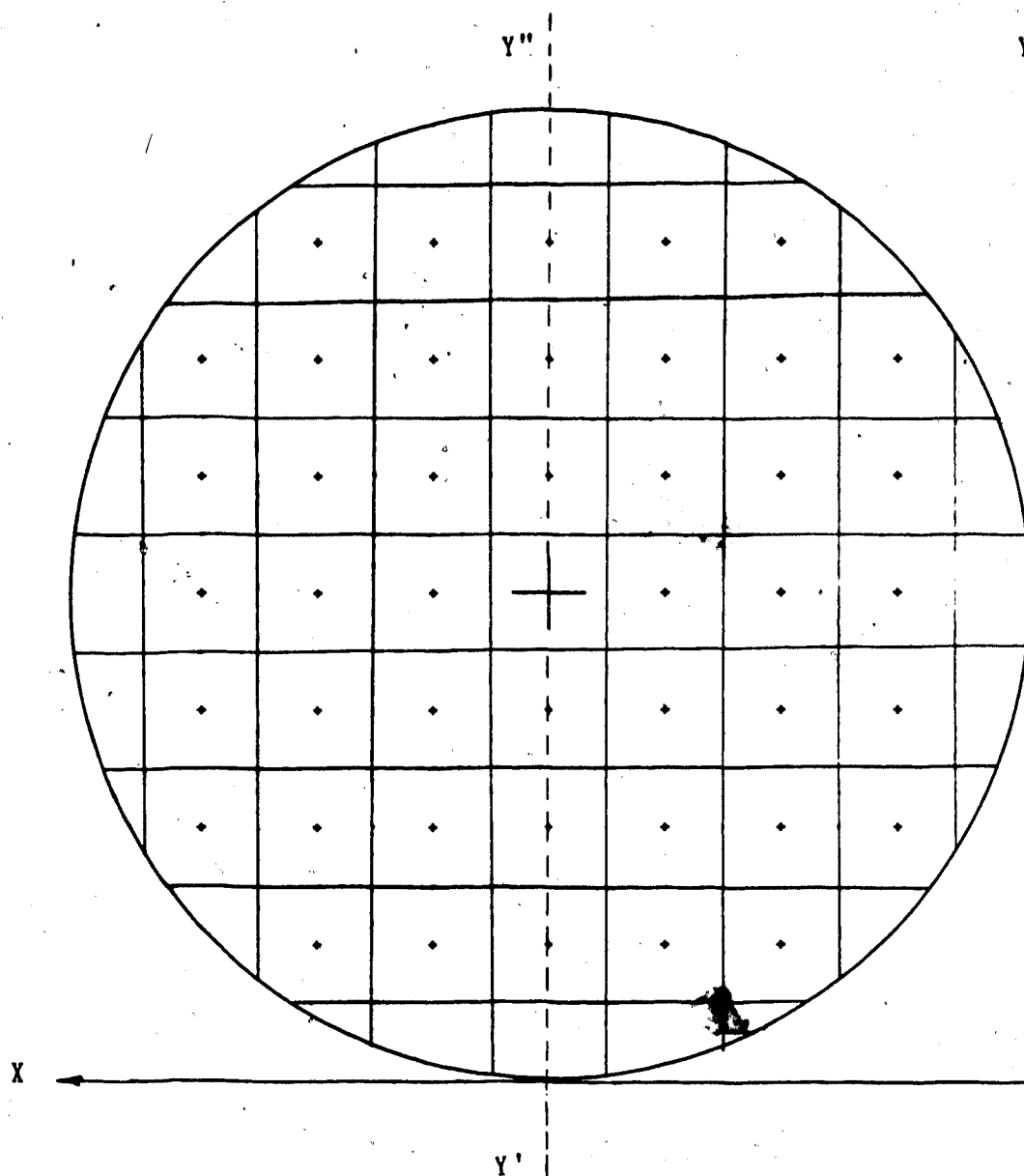


Figure 4.14 Grid system for LWC prediction.

attributed to the large grid size that was used. The potential for an accurate LWC profile exists in this program. More accurate results could be obtained if a smaller grid size is used.

#### 4.4 Comparison of Wind Tunnel Characteristics

##### (Batchelor & Shaw Versus Cubic Equation Type)

This program has been used to analyse the performances of wind tunnels with different contraction shapes. How the geometrical shape of the contraction section affects the thermodynamic and dynamic equilibrium and focusing effect can be studied using this program. By using this kind of study the choice of the type of wind tunnel which is best suited for different situations can be made before construction.

The two different contraction shapes analysed were the Batchelor and Shaw type (E.&C.) and Cubic Equation type (C.E.). Both are candidates for a marine icing wind tunnel to be constructed at the Mechanical Engineering Department at the University of Alberta. The profile of both types are shown in Figure 4.15. Each contraction was defined in one continuous equation as follows:

$$R = D_i/2 - 3/2(D_i - D_e)(x/L)^2 + (D_i - D_e)(x/L)^3 \quad (4.1)$$

$$1/R^4 = 1/R_i^4 + (1/R_e^4 - 1/R_i^4)(x/L - (\sin 2\pi x/L)/2) \quad (4.2)$$

Both equations describe the radius of the contraction at a distance 'x' from the inlet and 'L' is the length of the contraction. The subscripts 'i' and 'e' refer to inlet

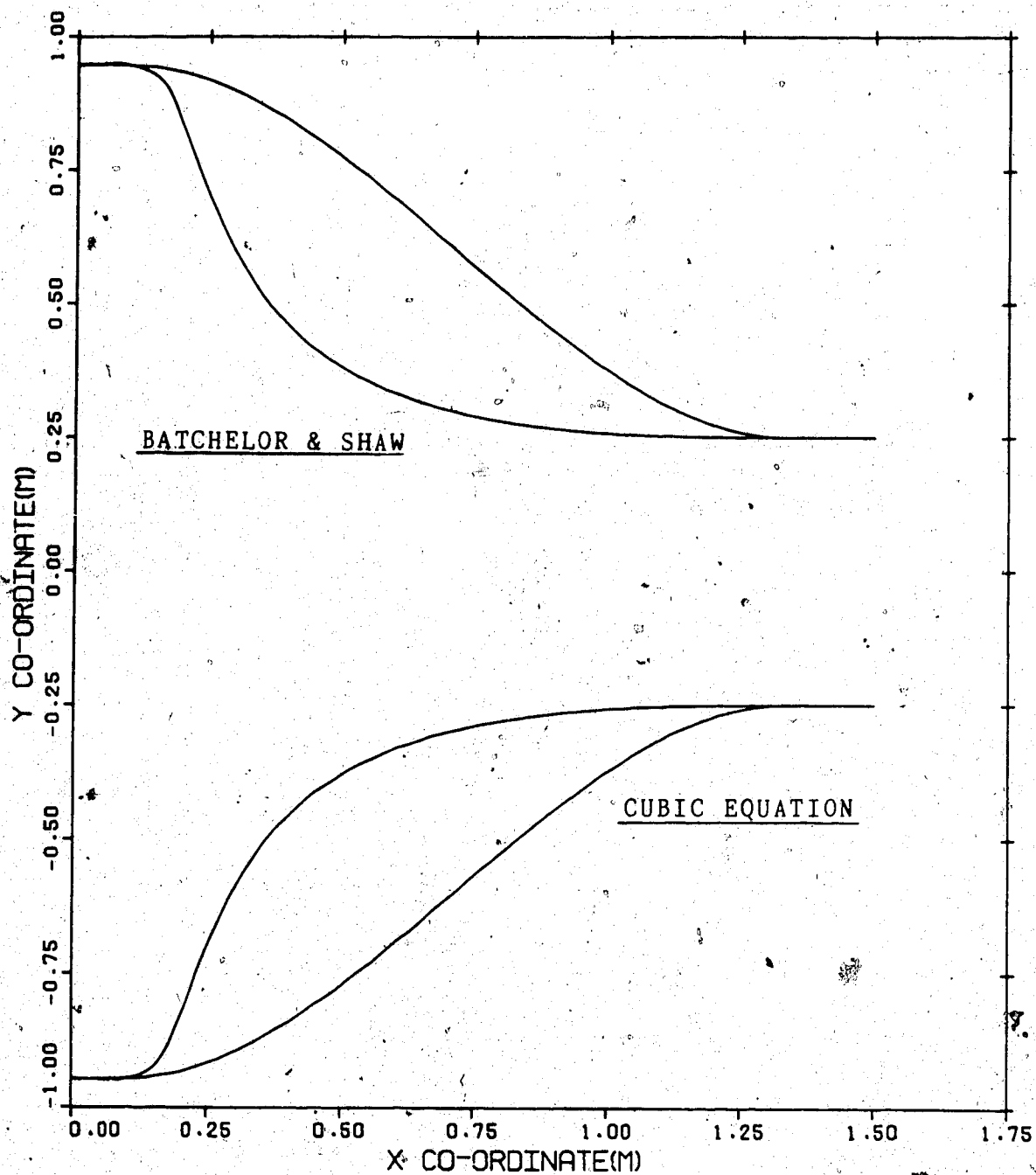


Figure 4.15 Profile of Batchelor & Shaw type and Cubic Equation type contractions.

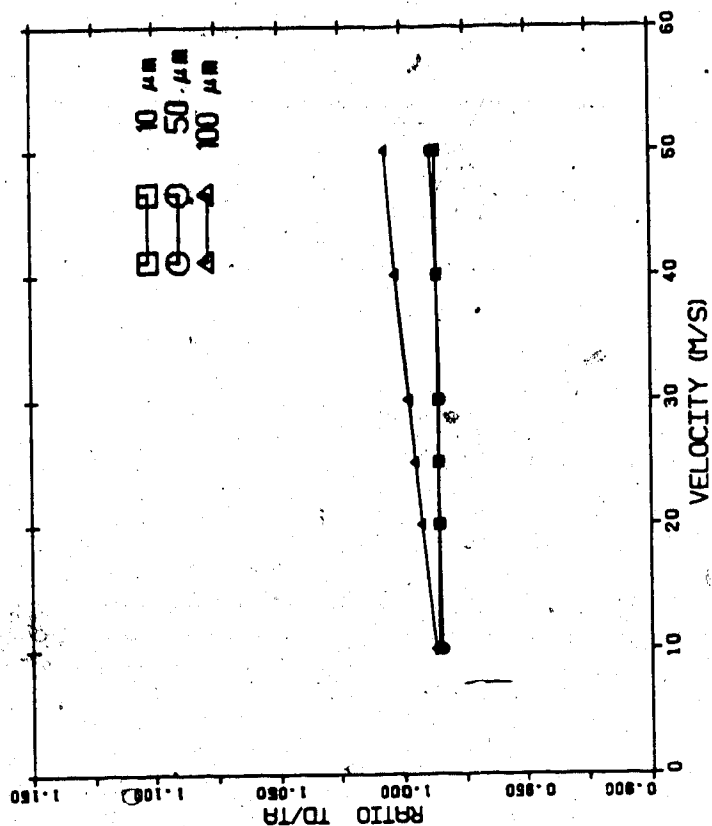


and outlet radii of the contractions. Equation 4.1 is for C.E. type tunnel while Equation 4.2 is for B.&S. type tunnel. Both types of wind tunnels are assumed to have circular cross sections. The two wind tunnels have the same contraction ratio of  $(3.75)^2$  and total length of 1.25 metres. As can be seen from Figure 4.15, the main difference between these two types of wind tunnels is the geometrical shape. The B.&S. type has a sharp contraction whereas C.E. type has a smoother contraction. The difference in performance due to the geometrical shape was therefore examined in the present study.

A comparison of the thermodynamic and dynamic equilibrium of the droplets for the two types of wind tunnels is shown in Figures 4.16 and 4.17. Again droplet sizes of 10 microns, 50 microns, and 100 microns were used. The value of test section speeds used was increased to include 10m/s, 20m/s, 25m/s, 30m/s, 40m/s, and 50m/s. The vertical and horizontal scales for dynamic and thermodynamic equilibrium comparison are similar to those used earlier.

According to Figure 4.16, it was found that for the three different droplet sizes, the thermodynamic equilibrium curves for the C.E. type are always below the curves of the B.&S. type. The relative humidity for these results was specified at zero, which causes the equilibrium ratio to be much less than one; that is, the final droplet temperature is lower than the air temperature. From these results it can be concluded that the C.E. type has a better geometric shape

# CUBIC EQUATION



# BATCHELOR & SHAW

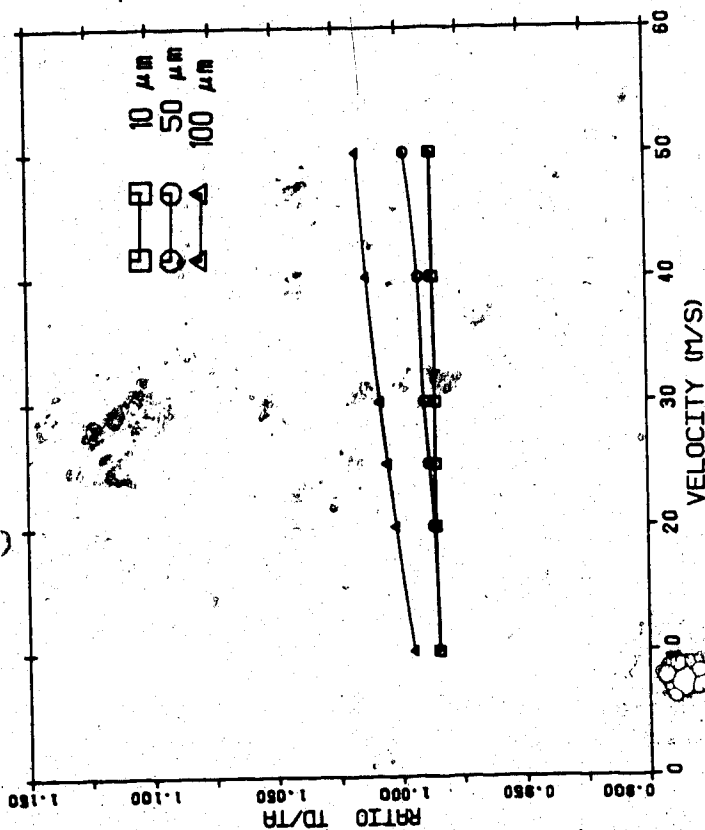


Figure 4.16 Comparison of thermodynamic equilibrium.

for thermodynamic equilibrium.

For dynamic equilibrium comparison, as shown in Figure 4.17, it was found that apart from 10 micron droplet, both types have not achieved equilibrium; however, the equilibrium curves for B.&S. type are much closer to the equilibrium than the C.E. type. Based on these results we can conclude that the B.&S. type provides better dynamic equilibrium for the droplets than the C.E. type.

These performance results can be explained in a similar fashion as the results for the FROST tunnel. We can look at the duration the droplets spend inside the wind tunnel, the total heat transfer rate, the momentum transfer and analyse the geometric shape of the tunnels. As shown in Figure 4.15, the B.&S.'s steeper contraction allows the droplets to arrive at the final cross section sooner than the C.E. type. For the same tunnel length, the B.S. type has a longer portion which is at the final cross section dimension. This would mean that the droplets stayed at the final velocity longer for the B.&S. type than for the C.E. type. Consequently, the droplets arrived at the end of the wind tunnel with a velocity closer to that of the free stream. Using the same argument, we can say that the droplets travel at a higher average velocity which means they spent less time inside the wind tunnel. This resulted in a decrease in heat transfer. The temperature of the droplet for the C.E. type is closer to the equilibrium temperature than that of the B.&S. type. Even though the

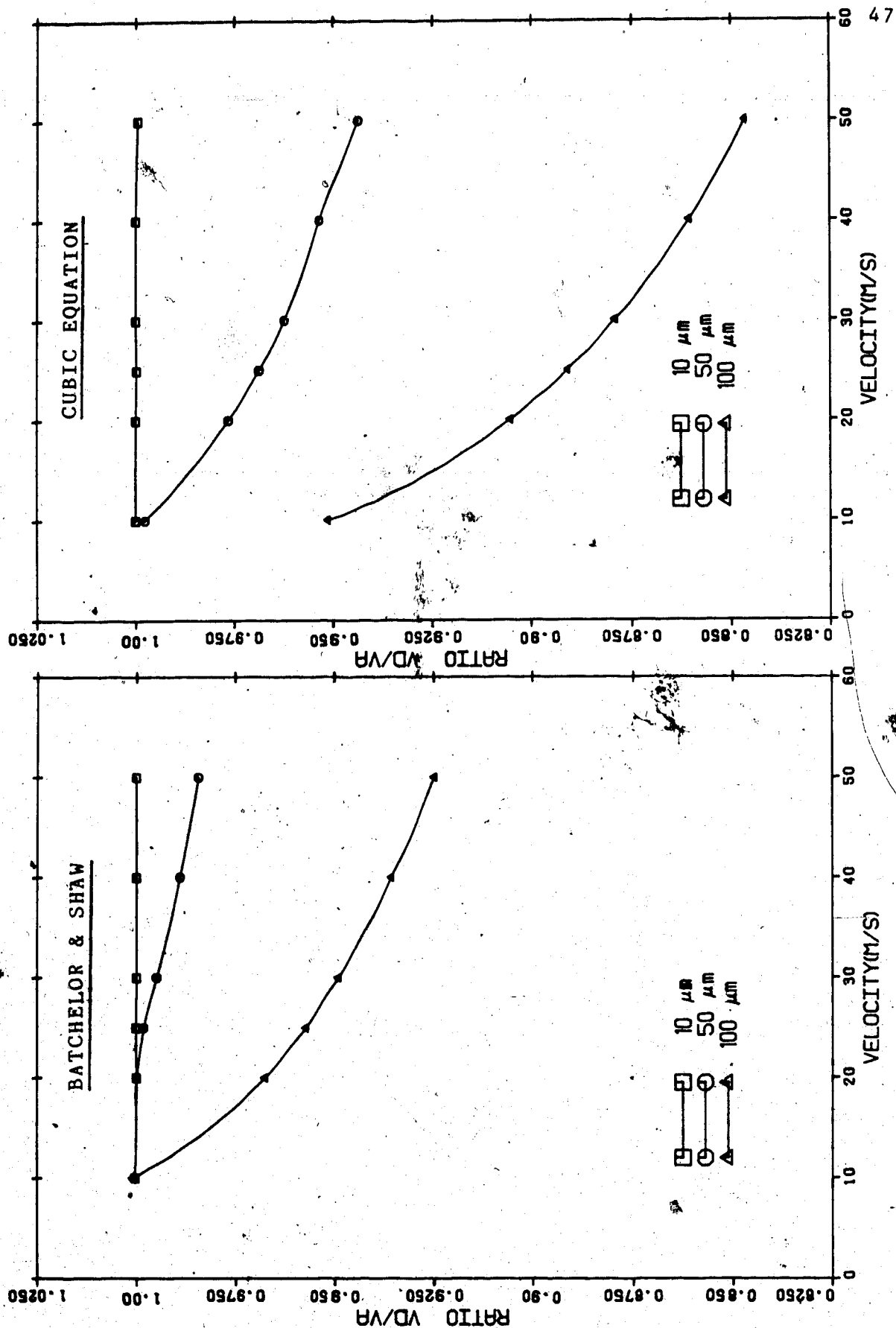


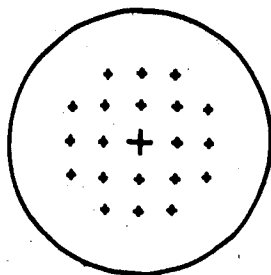
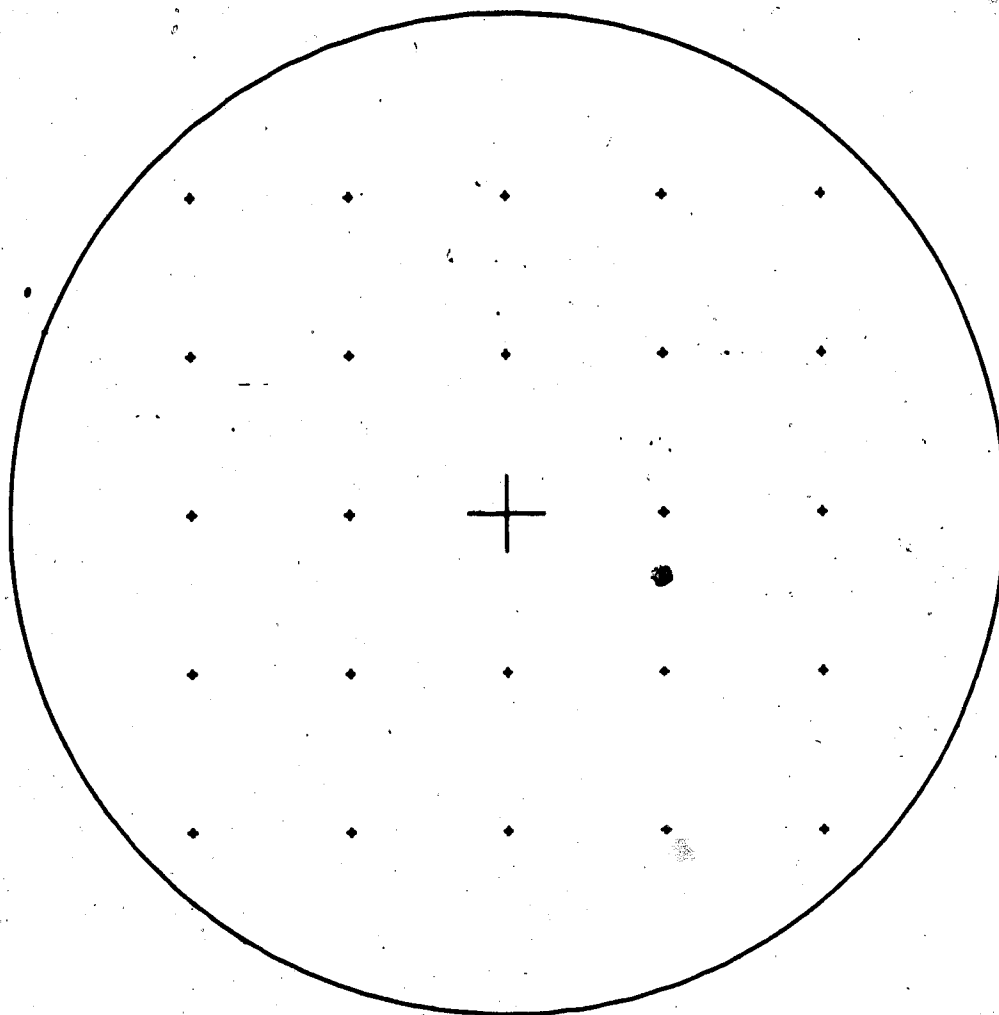
Figure 4.17 Comparison of dynamic equilibrium.

convective heat transfer is larger for the former type because of the larger difference in velocity, as explained earlier, the increase in the rate of convective and evaporative heat transfer do not compensate for the decrease in total time inside the tunnel contraction.

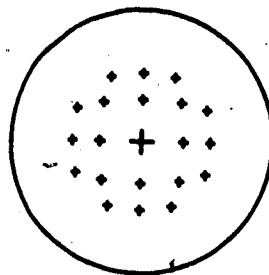
#### 4.5 Comparison of Focusing Effect

Figures 4.17 and 4.18 show the comparison of focusing effect between the two types of contractions for 100 micron droplets at test section speeds of 10m/s and 25m/s respectively. The left hand side is the initial grid for the droplets at the inlet of the tunnel. The right hand side are the positions of the droplets at the outlets of the two contractions. Droplets at the four corners of the grid are not shown because they disappeared due to collision with the contraction wall. The contraction was modelled with the central axis in the vertical orientation. Therefore, the gravitational force was acting in the direction of travel.

As can be seen in figure 4.17, the final position of the droplets for the B.&S. type is closer together than the C.E. type. This comparison in focusing effect is more obvious at a higher test section speed of 25m/s, as shown in Figure 4.18. Hence, it can be concluded that the B.&S. type has a stronger focusing effect. It would imply that the B.&S. type provides a higher LWC at the centre of the cross section. While the C.E. type provides a more even LWC distribution across the cross section. This can be explained

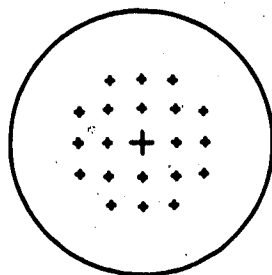
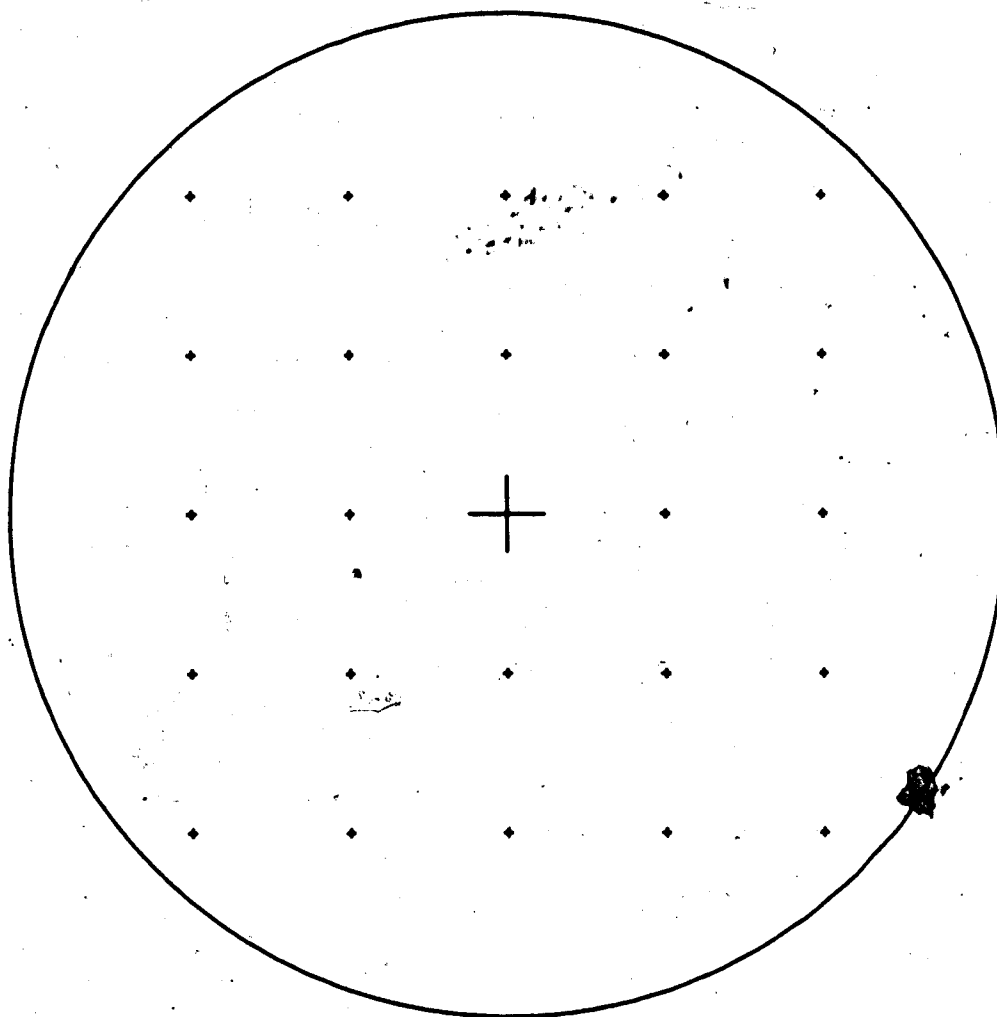


CUBIC EQUATION

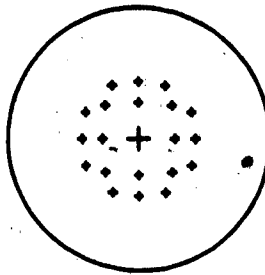


BATCHELOR AND SHAW

Figure 4.18 Comparison of focusing effect at a test section speed of 10 m/s.



CUBIC EQUATION



BATCHELOR AND SHAW

Figure 4.19 Comparison of focusing effect at a test section speed of 25 m/s.

by looking at the two contraction shapes. The C.E. type has a gently sloping contraction and therefore allows the droplets to pass through without deflecting the trajectories. While the B.&S. type's steep contraction caused the droplets to follow its contour.

#### 4.6 Comparison of One-dimensional Predictions and Axi-symmetric Predictions

The algorithm developed by Auld (1980) is limited to predicting droplet properties of droplets travelling in a test facility which are described by a one-dimensional profile. However, it is more efficient compared to the axi-symmetric program which provides more accurate flow characteristics for the wind tunnel and is more versatile in predicting the droplet properties. It is of interest in this study to determine how the predictions of the droplet properties differ between these two programs. The comparison was based on the predictions obtained for the FRCST wind tunnel. Results for two droplet sizes, 25 microns and 100 microns, and three test section speeds of 10m/s, 25m/s, and 50m/s were used for comparison.

The trajectories for the one-dimensional program were assumed to be a straight line from the centre of the inlet to the centre of the outlet. However, for the axi-symmetric program the droplet trajectories are governed by gravity and the focusing effects of the wind tunnel. In order to obtain some results that are comparable, the droplets were



introduced at the centre of the inlet, but in most cases the droplets did not end up at the centre of the outlet due to the gravity effect.

It was found that the final droplet temperatures obtained from the one-dimensional program were always lower than that from the axi-symmetric program. A consistent difference of 2 K was recorded. The final droplet velocity differed very little in most cases. A difference of less than one percent was recorded. It was also found that the time duration of the droplets inside the icing tunnel contractions was different. The time for the droplet to travel the same distance was found to be longer for Auld's program. We can explain this by looking at the velocity profile at the contraction section. It was found that the axi-symmetric program produced a velocity profile which had a higher velocity than velocity close to the wall. Therefore, when compared to a uniform velocity profile, the droplets passed through the tunnel in a shorter time in the axi-symmetric program.

The small differences in predictions of the properties of the droplet by these two programs suggest that there is no advantage to using the more complex model. However, the axi-symmetric program can provide more information on the trajectory of the droplet, the focusing effect due to the contour of the wind tunnel, and the IWC across the wind tunnel and can also help predict the proper tunnel shape for certain type of application.

## Chapter Five

### Conclusions and Recommendations

The purpose of this study was to develop a computer algorithm that can be used to predict the trajectory and temperature of a droplet travelling inside any test facility which has an axi-symmetric cross section. The program predicts results such as the temperature and velocity of the droplet at any location along the wind tunnel. Since the program is a two-dimensional model, it can also determine the gravity effect, and the focusing effect due to the contraction shape of the test facility. With this information, the final location of the droplet can be determined. Therefore, this program can be used as a design tool for wind tunnel construction. Another objective of this study was to find out the equilibrium of the droplet properties with respect to the air properties. These results can be used in the icing programs which predict the amount of icing accumulated on objects.

The algorithm is written in FORTRAN. Because of the complexity of the algorithm it is divided into three parts: FLOW, MAIN and LIBSUB. FLOW calculates the flow pattern inside the testing facility. MAIN calculates the trajectory and temperature of the droplet. LIBSUB is a compilation of the library subroutines used by both FLOW and MAIN.

A parameteric study was performed on the equilibrium of the droplets travelling inside the FROST icing wind tunnel in the Mechanical Engineering Department at the University of Alberta. Droplet sizes of 10 microns, 50 microns and 100 microns, test section speeds of 10m/s, 25m/s and 50m/s were used in the present study. It was found that for a 10m/s test section speed, the droplets achieved equilibrium both dynamically and thermodynamically for the three droplet sizes. Equilibrium was also achieved for 10 micron droplets at test section speeds up to 50m/s. However, for bigger droplets, 50 microns and 100 microns, equilibrium was not achieved at test section speeds higher than 10m/s. The deviation between the droplet and air properties increased as the droplet size and test section speed increased.

An attempt was made to determine the liquid water content across the test section. However, the grid size used was too large and the results do not match some experimental results. It is recommended that a smaller grid size be used. However, some information on the focusing and gravity effect on the droplets were produced using this grid size. It was found that at high test section speeds the focusing effect was more dominant than the gravity effect. At low test section speeds the reverse is true. Also, small droplets are more susceptible to the focusing effect while larger droplets are more susceptible to gravity effects.

A performance test was made between two wind tunnels with different contraction shapes. They were the Batchelor and Shaw Type (B.&S.) and Cubic Equation Type (C.E.). The B.&S. type has a steeper contraction shape and the C.E. type has a smoother contraction shape. It was determined that for the same tunnel length, the B.&S. type is more suitable for obtaining dynamic equilibrium for the droplet, while the C.E. type is more suitable for thermodynamic equilibrium.

A comparison was made between the results obtained using the one-dimensional program by H.E. Auld and the axi-symmetric program. It was determined that the final droplet speed from both programs were almost identical. However, the droplet temperatures from Auld's one-dimensional program were always two degrees Kelvin lower than the axi-symmetric program. Based on this result, the one-dimensional program could be used to calculate droplet properties in most cases. It is recommended that the axi-symmetric program be used if, for example, the trajectory of the droplet is also required. This program can also be used as a design tool to analyse the performance of different type of wind tunnels to determine the proper shape of the contraction before construction.

## REFERENCES

- AULD, H.E., 1980: The Thermodynamics of Icing Sprays. M.Sc. Thesis, Dept. of Geography, Univ. of Alberta.
- BEARD, K.V. AND PRUPACHER H.R., 1971: A Wind Tunnel Investigation of The Rate of Evaporation of Small Water Drops falling at Terminal Velocity in Air. J.Atmos.Sci., V-28, 1455-1464.
- BEARD, K.V. and PRUPPACHER, H.R., 1969: A Determination of The Terminal Velocity and Drag of Small Water Drops by Means of A Wind Tunnel. J. Atmos. Sci., V-26, P-1066-1072.
- GATES, E.M. and LOZOWSKI, E.P., 1984: Ice Accretion on Structures in a Marine Environment. ASME PET-2.
- JOE, P.I., 1975: Investigation of the Bouncing of Supercooled Water Droplets from an Artificially Growing Hailstone. M.Sc. Thesis, Dept. of Physic, Univ. of Toronto, 254p.p.
- KELLOG, O.D., 1929: Foundations of Potential Theory. Frederick Unger Publishing Company. Also Dover Publications Inc.
- LeCLAIR, B.P., HAMIELLEC, A.E. and PRUPPACHER, H.R., 1970: A Numerical Study of the Drag on a Sphere at Low and Intermediate Reynolds Numbers. J. Atmos. Sci., V-27, 308-315.
- LOWE, P.R., "An Approximating Polynomial for the Computation of Saturated Vapour Pressure", J. Appl. Meteor., Vol. 16, p.100-103, 1977.
- OLESKIW, M. M. 1982: A Computer Simulation of Time-dependent Rime Icing on Airfoils: Ph.D. Thesis, Dept. of Geography, Univ. of Alberta.
- PRUPPACHER, H.R. and KLETT, J.D., 1978: Microphysics of Clouds and Precipitation. Dordrecht, Holland, D. Reidel Publishing Company, 656 pp.
- SMITH, A.M.O. and PIERCE, J., 1958: Exact Solution of Neumann Problem. Calculation of Non-circulatory Plane and Axially Symmetric Flows About or Within Arbitrary Boundaries. Douglas Aircraft Company Report #ES 26988.

## APPENDIX A

### Flow Field Calculation Details

The following is the detailed derivation of the equations used to calculate the flow inside axi-symmetric wind tunnels.

### A.1 Calculation of the flow field

Neumann's method was originally developed for flow over two-dimensional bodies to calculate low speed non-circulatory flows about or within bodies. The similarities between two dimensional bodies and axially symmetric bodies lead to further development which is used for solving flow over axially symmetric bodies. The general theory for flow over bodies is presented here. This generalization also applies to flow inside the wind-tunnel with an axially symmetric profile.

The notation and measuring system are shown in Figure A.1 which shows the cross-section of an axially symmetric body. The body is described by an arbitrary number of co-ordinates points on a meridian curve in a Cartesian Co-ordinate system. Based on these points, the body is made up by a series of elements of frustums. By using Neumann's method, a set of source densities for the elements can be calculated, thus providing the body surface with a continuous distribution of source densities. The velocity potential at a point 'P<sub>2i-1</sub>' due to the ring sources can be calculated according to the following equation:

$$\phi(P) = \iint_S \frac{\sigma(q)ds}{L} \quad (A.1)$$

The surface integral involves ' $\sigma$ ' the surface density at a point 'Q' on the body and 'L' the distance between 'P' and 'Q'.

According to potential theory, the directional





derivative of the velocity potential is the velocity in that direction. Therefore, the directional derivative of Equation A.1 is:

$$\frac{\partial \psi}{\partial n_-}(P) = 2\pi\sigma(P) + \iint_S \sigma(q) \frac{\partial}{\partial n} \frac{1}{L} ds \quad (A.2a)$$

$$\frac{\partial \psi}{\partial n_+}(P) = -2\pi\sigma(P) + \iint_S \sigma(q) \frac{\partial}{\partial n} \frac{1}{L} ds \quad (A.2b)$$

where '+' sign represents the inward direction and the '-' sign represents the outward direction. Point 'P' is on the body and the value of ' $2\pi\sigma$ ' is missing during the surface integration. All points on the surface of the body involve ' $2\pi\sigma$ ' value and this value has been included in Equations A.2a and A.2b. The explanation for this is included in most potential treatises such as Kellogg (1929) and will not be dealt with here. Directional derivatives are usually obtained for the X and Y direction in the Cartesian co-ordinate system. Velocity in other directions can be obtained by combining these velocity components.

The set of surface densities can be solved by using the following procedure. First, we determine the left hand side of Equation A.1. This is the boundary condition of the problem and is specified as the velocity at the midpoint of the frustum. Most boundary conditions are for solid bodies; that is, the normal velocity through the surface is zero. The boundary condition can be specified for permeable

surfaces also, which have variable amounts of flow. The next procedure is to calculate the surface integral on the right hand side of the equation. This is accomplished by summation according to Simpson's rule. In order to use this summation method, each major element has to be subdivided into even number of subelements. The total number of subelements is inversely proportional to the distance between point 'P' and 'Q'. A problem exists when 'P' and 'Q' are the same point, because 'L' becomes zero and the integral is infinity. In this case a singularity exists and the integral must be calculated analytically by means of a power series. The details are explained in Section A.3

For 'n' numbers of elements there are 'n' number of midpoints and 'n+1' numbers of co-ordinate points. The midpoint is specified as the location where the boundary condition of each ring exists. This point is influenced by all the ring sources of the body; therefore, n number of simultaneous equations are formed. The set of n number of unknown source densities is obtained by solving these simultaneous equations using numerical methods. Once the set of surface densities is known, values of the potential and its derivatives, in any directions, can be calculated.

There is no restriction to the number of elements that can be used to represent the bodies. Generally, a larger number of elements gives more accurate results but also means higher computer costs.

## A.2 Velocity Potential and Velocity Induced by a Ring Source

For ease of representation a thin wire source ring of radius 'a' with linear density ' $\lambda$ ' is used to establish the expressions for the velocity potential and its derivatives at point 'P'. The centre of the ring is taken as the origin. Point 'P' lies in the vertical plane (see Figure A.2) and its co-ordinates in the Cartesian system are (x, y, 0). Point 'Q' is a general point on the ring with co-ordinates (0, a cos  $\theta$ , a sin  $\theta$ ). Hence, 'L' the distance between 'P' and 'Q' is:

$$\begin{aligned} L^2 &= x^2 + (y - a \cos \theta)^2 + a^2 \sin^2 \theta \\ &= x^2 + y^2 + a^2 - 2ay \cos \theta \end{aligned} \quad (\text{A.3})$$

According to Equation A.1 the velocity potential at point 'P' due to the entire ring source is:

$$(\psi)_P = \int_0^{2\pi a} \frac{\lambda ds}{L} \quad (\text{A.4})$$

Since 'a' and ' $\lambda$ ' are constant and due to the symmetry of the geometry, Equation A.4 can be reduced to:

$$(\psi)_P = 2 \lambda a \int_0^\pi \frac{d\theta}{L} \quad (\text{A.5})$$

Now substituting Equation A.3 into Equation A.5 gives:

$$(\psi)_P = 2 \lambda a \int_0^\pi \frac{d\theta}{\sqrt{x^2 + y^2 + a^2 - 2ay \cos \theta}} \quad (\text{A.6})$$

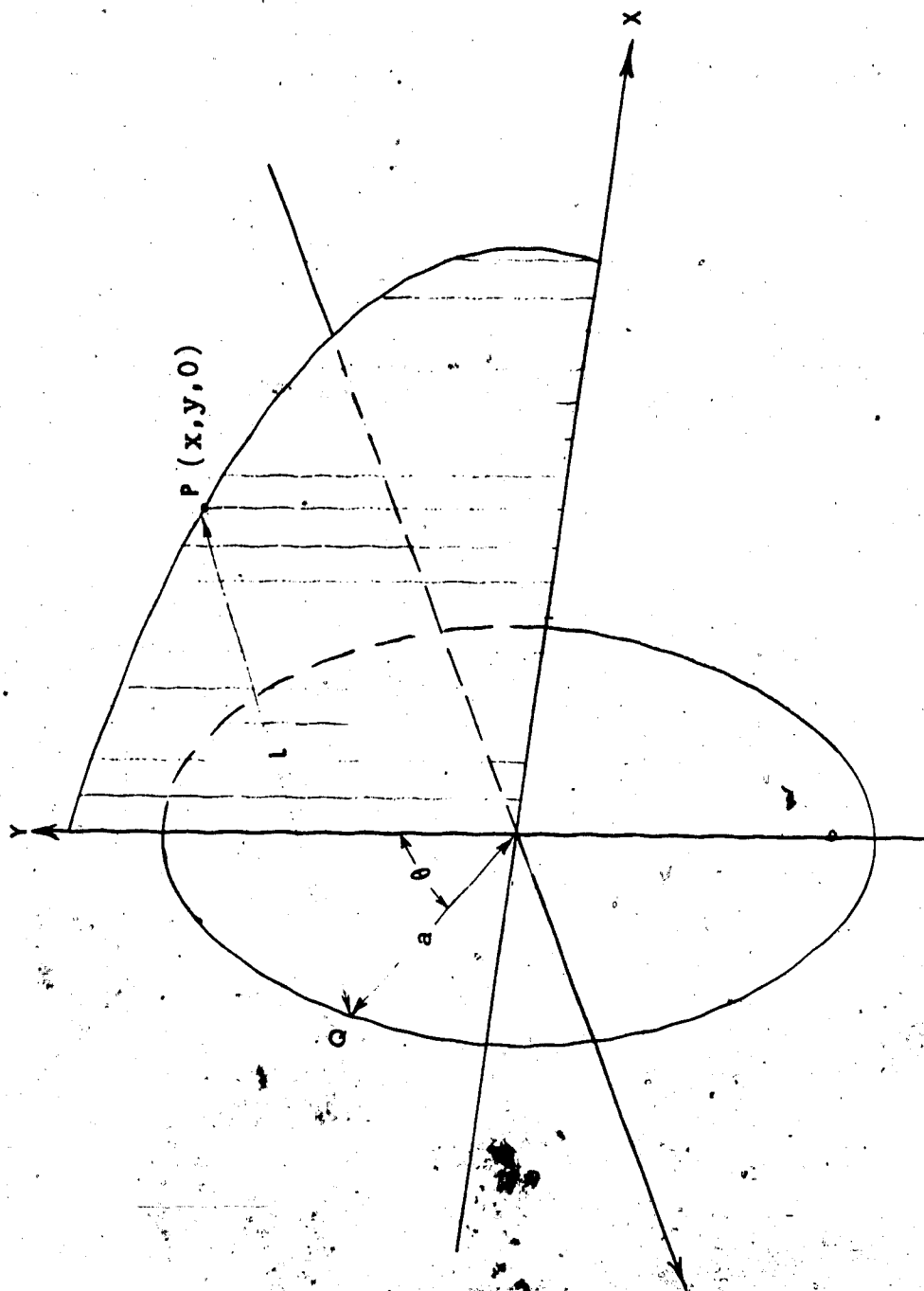


Figure A.2 Analysis of velocity potential due to a circular ring source.

Therefore, the derivatives of the velocity potential in the X and Y directions are:

$$\left(\frac{\partial \psi}{\partial x}\right)_p = -2a\lambda \int_0^\pi \frac{x \, d\theta}{(x^2 + y^2 + a^2 - 2ay \cos \theta)^{3/2}} \quad (\text{A.7a})$$

$$\left(\frac{\partial \psi}{\partial y}\right)_p = -2a\lambda \int_0^\pi \frac{(y - \cos \theta) d\theta}{(x^2 + y^2 + a^2 - 2ay \cos \theta)^{3/2}} \quad (\text{A.7b})$$

The basic expressions for the principal velocity have to be converted to a more useful form so that the integration can be performed numerically. The conversion requires algebraic and trigonometric manipulation of Equations A.7a and A.7b. The details of the transformation are given in A.M.O. Smith (1958) and only the final forms are shown here.

$$\left(\frac{\partial \psi}{\partial x}\right)_p = \frac{-4a\lambda x E(k)}{[\sqrt{(y+a)^2 + x^2}][\sqrt{(y-a)^2 + x^2}]} \quad (\text{A.8a})$$

$$\left(\frac{\partial \psi}{\partial y}\right)_p = \frac{-2a\lambda}{y\sqrt{(y+a)^2 + x^2}} \left[ K(k) + \frac{y^2 - a^2 - x^2}{(y-a)^2 + x^2} E(k) \right] \quad (\text{A.8b})$$

$$k^2 = \frac{4ay}{(y+a)^2 + x^2} \quad (\text{A.8c})$$

where  $E(k)$  is the elliptical integral of the First Kind and  $K(k)$  is the elliptical integral of the Second Kind.

The above expressions are for a ring element located at the origin. The expressions for an element located at an arbitrary position 'b' along the X-axis and the linear source density ' $\lambda$ ' is replaced by ' $\sigma \delta S$ ', where ' $\sigma$ ' is the surface density and ' $\delta S$ ' is the thickness of the element, are modified as follows

$$\delta \left( \frac{\partial \phi}{\partial x} \right)_p = \frac{-4a(x-b)\sigma\delta S E(k)}{\sqrt{(y+a)^2 + (x-b)^2} [(y-a)^2 + (x-b)^2]} \quad (A.9a)$$

$$\delta \left( \frac{\partial \phi}{\partial y} \right)_p = \frac{-2a\sigma\delta S}{y\sqrt{(y+a)^2 + (x-b)^2}} \left[ k(k) + \frac{y^2 - a^2 - (x-b)^2}{(y-a)^2 + (x-b)^2} E(k) \right] \quad (A.9b)$$

$$k^2 = \frac{4ay}{(y+a)^2 + (x-b)^2} \quad (A.9c)$$

### A.3 Calculation for Singular Subelements

As mentioned earlier, the surface integral of Equation A.1 becomes infinity when 'P' coincides with 'Q'. Equation A.9 cannot be used for this singular subelement and is dealt with in the following manner. Figure A.3 is a frustum which represents the ring source of the centre subelement. The slant height is equal to,  $2s'$ . Point 'P' is the midpoint on the surface of the frustum. Since 'P' is on the surface of the bodies, which is not a general point, the contribution of ' $2\pi\sigma$ ' to the derivatives of the potential is missing. For ease of operation, this missing

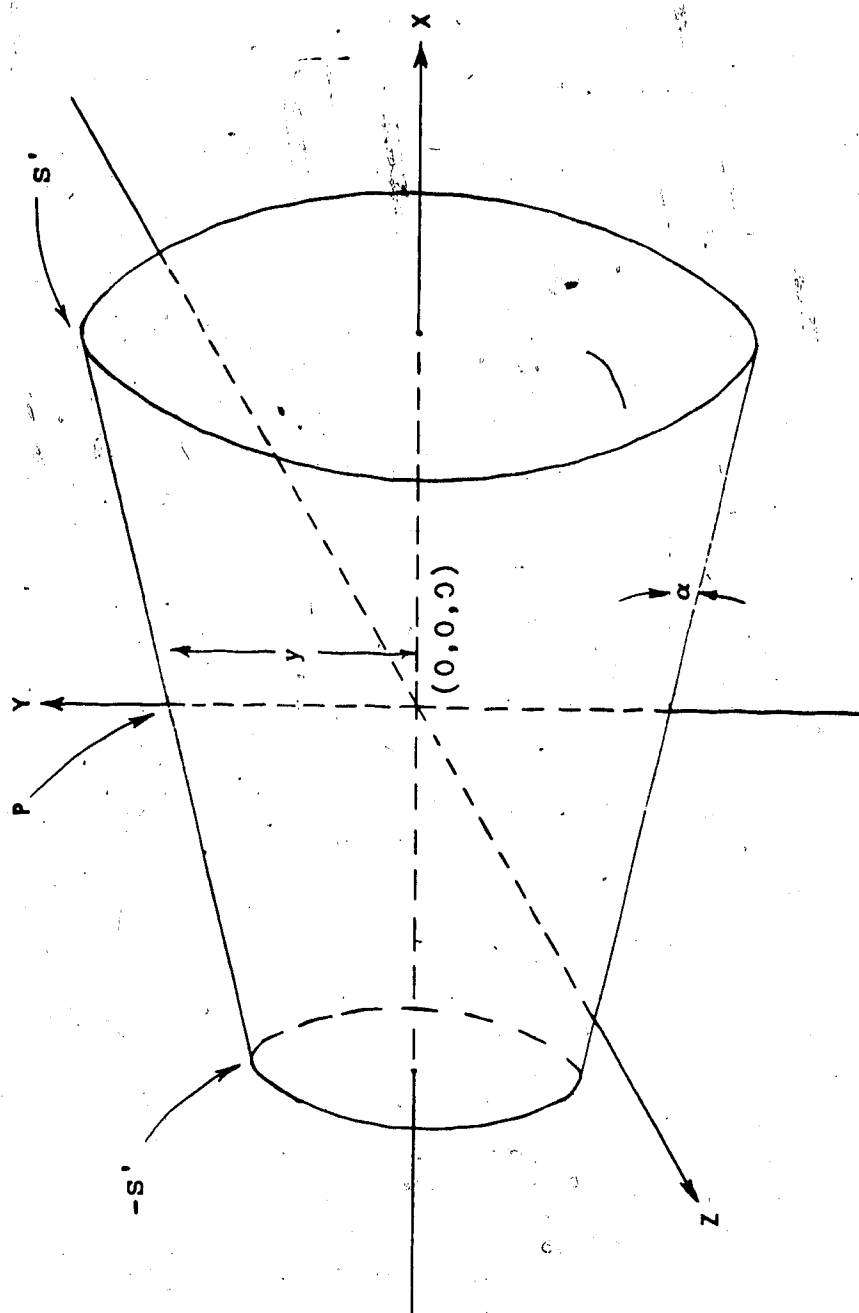


Figure A.3 Analysis of velocity potential due to a singular subelement.

quality is not dealt with here but will be added later.

As seen in the Figure A.3, 'P' is a point directly above the origin therefore its co-ordinates are (0, y, 0) and the rest of the variables are

$$X = 0$$

$$Y = \text{constant}$$

$$a = y + S \sin \theta$$

$$b = a \cos \theta$$

The expressions can now be integrated analytically. If the ratio (fineness ratio)  $s'/y$  is not greater than 0.008, the elliptic integrals can be expressed as the sum of a power series plus a second power series multiplied by a logarithmic term. It must be cautioned that the accuracy decreases as the fineness ratio  $s'/y$  increases. If all the variables are substituted into Equations A.9a, A.9.b and A.9.c the following expressions are formed:

$$\left(\frac{\partial \phi}{\partial x}\right)_p^1 = 4 \sigma \cos \alpha \int_{-S'}^{S'} \frac{(1 + s/y \sin \alpha) E(k)}{\sqrt{(4 + 4 s/y \sin \alpha) + (s/y)^2}} \frac{ds}{S} \quad (\text{A.10a})$$

$$\left(\frac{\partial \phi}{\partial y}\right)_p^1 = \int_{-S'}^{S'} \frac{-2\sigma(1 + s/y \sin \alpha)}{4 + 4 s/y \sin \alpha + (s/y)^2} \left[ K(k) - \frac{(s/y + 2 \sin \alpha) E(k)}{s/y} \right] \frac{ds}{y} \quad (\text{A.10b})$$

$$k^2 = \frac{4y(y + S \sin \alpha)}{4y^2 + 4sy \sin \alpha + S^2} \quad (\text{A.10c})$$

The superscript '1' denotes the integral is for the



singular point. The expressions are now ready to be integrated analytically. Details of the procedure is presented in A.M.O. Smith (1958) and only the final form of the expressions are given here.

$$\left(\frac{\partial\psi}{\partial x}\right)_p^1 = \sigma \sin \alpha \cos \alpha \left[ 2S^1 + \left(\frac{13}{72} + \frac{1}{12} \ln \frac{S^1}{8} + \frac{1}{12} \sin^2 \alpha\right) S^{1^3} + \dots \right] \quad (\text{A.11a})$$

$$\left(\frac{\partial\psi}{\partial y}\right)_p^1 = \sigma \left[ (2 \sin^2 \alpha + 2 \ln S^1/8) S^1 - \frac{1}{24} (3 + 3 \ln \frac{S^1}{8} - 3 \sin^2 \alpha - 2 \sin^4 \alpha) S^{1^3} + \dots \right] \quad (\text{A.11b})$$

The missing value of ' $2\pi\sigma$ ' can now be added to the expression above. The following are the expressions for the velocity components for point 'P' after the components of ' $2\pi\sigma$ ' are added

$$\left(\frac{\partial\psi}{\partial x}\right)_+ = 2\pi \sigma_+ \sin \alpha + \left(\frac{\partial\psi}{\partial x}\right)_+^T \quad (\text{A.12a})$$

$$\left(\frac{\partial\psi}{\partial y}\right)_+ = -2\pi \sigma_+ \cos \alpha + \left(\frac{\partial\psi}{\partial y}\right)_+^T \quad (\text{A.12b})$$

superscript 'T' denotes the total contribution of the entire element.

Equations A.11a and A.11b are used only when Equations A.9a and A.9b cannot be used, that is, when 'P' equals 'Q'. The necessary formulae are now available for determining the derivatives of the velocity potential in any direction and at any point on the body. With these formulae, a system of equations can be constructed, so that the unknown values of the surface density can be solved.

#### A.4 Formulation of the Equations for Solving the Values of the Set of Source Densities

The following procedure describes the construction of the set of equations to calculate the surface densities on the body. For clarity, elements will be identified in the following manner. For the point of interest 'P', letter 'i' is used, and for the variable point of integration 'Q', letter 'j' is used. Points on the frustums are described by 'P<sub>2i-2</sub>' and 'P<sub>2i</sub>' for the end points, and 'P<sub>2i-1</sub>' for the midpoints (see in Figure A.1). For calculations, these points in Cartesian Co-ordinates system are represented by ( $\xi_{2i-2}$ ,  $\eta_{2i-2}$ ), ( $\xi_{2i}$ ,  $\eta_{2i}$ ) and ( $\xi_{2i-1}$ ,  $\eta_{2i-1}$ ) respectively. For the  $i=j$  frustum, ' $\xi$ ' and ' $\eta$ ' are represented by 'b' and 'a'.

In order to help organize and understand the set of equations, the quantities ' $X_{ij}$ ' and ' $Y_{ij}$ ' are introduced. The derivatives of the velocity potential at any point 'P<sub>2i-1</sub>' influenced by the 'j' element is:

$$\left(\frac{\partial \phi}{\partial x}\right)_{ij}^A = \sigma_j X_{ij} \quad (A.13a)$$

$$\left(\frac{\partial \phi}{\partial y}\right)_{ij}^A = \sigma_j Y_{ij} \quad (A.13b)$$

where the superscript 'A' denotes all of the elements on the body. The expressions for ' $X_{ij}$ ', ' $Y_{ij}$ ' are determined solely by the geometry of the body. These expressions apply to two situations:  $i \neq j$  and  $i=j$ .

For the case when  $i \neq j$ , the following expressions,

which is obtained according to Equations A.9a and A.9b, are used.

$$x_{1j} = -4 \int_{S_{2j-2}}^{S_{2j}} \frac{\eta_j (x_{2i-1} - \xi_j) E(k) ds}{\sqrt{(y_{2j-1} + \eta_j)^2 + (x_{2j-1} - \xi_j)^2} [(y_{2i-1} - \eta_j)^2 + (x_{2i-1} - \xi_j)^2]} \quad (\text{A.14a})$$

$$y_{1j} = -2 \int_{S_{2j-2}}^{S_{2i}} \frac{\eta_1}{y_{2i-1} \sqrt{(y_{2i-1} + \eta_j)^2 + (x_{2i-1} - \xi_j)^2}} \left[ K(k) + \frac{y_{2i-1}^2 - \eta_j^2 - (x_{2i-1} - \xi_j)^2}{(y_{2i-1} - \eta_j)^2 + (x_{2i-1} - \xi_j)^2} E(k) \right] dS \quad (\text{A.14b})$$

For the case  $i=j$ , Equations A.9a, A.9b, A.13a and A.13b are required. The lengthy expressions are as follows. Here  $S_1 = S' / y_{2i-1}$  where  $S'$  is half of the length of the singular subelement. The equations are as follows:

$$x_{11} = \sin \alpha_1 \cos \alpha_1 \left[ 2 S_1 + \left( \frac{13}{72} + \frac{1}{12} \ln \frac{S_1}{8} + \frac{1}{12} \sin^2 \alpha_1 \right) S_1^3 + \dots \right]$$

$$I_X = -4 \int_{S_{2i-2}}^{(S_{2i-1}) - (S_1 y_{2i-1})} \frac{S_{2i}}{(S_{2i-1}) + (S_1 y_{2i-1})} I_X \quad (\text{A.15a})$$

where

$$I_X = \frac{\eta_1 (x_{2i-1} - \xi_1) E(k) dS}{\sqrt{(y_{2i-1} + \eta_1)^2 + (x_{2i-1} - \xi_1)^2} [(y_{2i-1} - \eta_1)^2 + (x_{2i-1} - \xi_1)^2]}$$

$$y_{11} = (2 \sin^2 \alpha_1 + 2 \ln \frac{S_1}{8}) S_1 - \frac{1}{24} [(3 + 3 \ln \frac{S_1}{8} - 3 \sin^2 \alpha_1 - 2 \sin^4 \alpha_1) S_1^3 + \dots]$$

$$- 2 \int_{S_{2i-2}}^{(S_{2i-1}) - (S_1 y_{2i-1})} I_y - 2 \int_{(S_{2i-1}) - (S_1 y_{2i-1})}^{S_{2i}} I_y \quad (A.15b)$$

where

$$I_y = \frac{\eta_i}{y_{2i-1} \sqrt{(y_{2i-1}^2 + \eta_i^2) + (x_{2i-1} - \xi_i)^2}} \left[ K(k) + \frac{(y_{2i-1}^2 - \eta_i^2 - x_{2i-1} - \xi_i)^2}{(y_{2i-1}^2 - \eta_i^2) + (x_{2i-1} - \xi_i)^2} E(k) \right] dS$$

By combining these 2 sets of equations, the derivatives of the potential at any points due to the entire body can be obtained. The integration in the expression is easily performed numerically by Simpson's rule, requiring division of each frustum into subelements. The values of the elliptical integrals  $E(k)$  and  $K(k)$  can be obtained by machine subroutines. The velocity, normal to the surface of the body at the midpoint of  $i$  frustum, can therefore be calculated by the following Equation A.16.

$$\left( \frac{\partial \phi}{\partial \eta_{2i-1}} \right) = 2\pi \sigma_i \sin \alpha_i \sum_{j=1}^n \sigma_j x_{ij} + \cos \alpha_i \sum_{j=1}^n \sigma_j y_{ij} \quad (A.16)$$

## APPENDIX B

### Listing of Programs

The following consists the listing of three programs. FLOW calculates the flow pattern inside wind tunnels. MAIN calculates the temperature, velocity and loaction of the droplets and LIBSUB is a compilation of the library subroutines used by FLOW and MAIN.

```

C*****
C
C PROGRAM : FLOW
C          -CALCULATION THE FLOW FIELD INSIDE A WIND
C TUNNEL.
C
C*****
C
C LIST OF VARIABLES :-
C LS      -MAXIMUM NUMBER OF SUBELEMENT ON THE FRUSTUM
C XM,YM   -MID POINT OF EACH FRUSTUM.
C LEN     -ACUMULATED LENGTH OF THE TUNNEL AT EACH FRUSTUM
C UINF    -ARBITRARY VELOCITY AT THE END OF THE TUNNEL.
C          THIS ACT AS A FORCING FUNCTION FOR CALCULATING
C          THE SOURCE DENSITY OF EACH FRUSTUM
C VF(I)   -ARRAY OF SOURCE DENSITY OF EACH FRUSTUM
C PX,PY   -POINT WHERE THE VELOCITY COMPONENTS ARE
C          CALCULATED
C XVEF    -X VELOCITY COMPONENT OF THE REQUIRED POINT
C
C*****

```

```

      REAL X(130),Y(130),LEN(130),XM(129),YM(129),NM(129),
      @      C(129),SINB(129),COSB(129),VF(129),VN(129,129),
      @      VT(129),XV(129,129),YV(129,129),VN1(129,129),
      @      XE,YE,BP,CBP,XI,YI,XF,YF,XMP,YMP,LENF,LENI,UINF
      @      PX,XVEF,YVEF,FX(250),FY(250)
      DIMENSION ICT(5)

```

```

C READ THE INPUT DATA
C-----

```

```

      READ (5,5) (ICT(I),I=1,5)
      READ (5,4) UINF
      READ (5,5) N,NS
      READ (5,2) (X(I),I=1,N)
      READ (5,2) (Y(I),I=1,N)

```

```

C PRINT OUT THE INPUT DATA
C-----

```

```

      WRITE (6,5) (ICT(I),I=1,5)
      WRITE (6,4) UINF
      WRITE (6,5) N
      WRITE (6,2) (X(I),I=1,N)
      WRITE (6,2) (Y(I),I=1,N)

```

```

      LS=10
      N1=N-1
      IFACT=2

```

C CALCULATE THE MID-POINT OF EACH FRUSTUM(TOTAL OF N-1)

C-----  
 DO 100 I=1,N1  
 $XM(I) = (X(I) + X(I+1)) / 2.0$   
 100  $YM(I) = (Y(I) + Y(I+1)) / 2.0$

C CALCULATE THE ACCUMULATED LENGTH OF THE TUNNEL

C-----  
 $LEN(1) = 0.0$   
 DO 101 I=1,N1  
 101  $LEN(I+1) = ((X(I+1) - X(I))^2 + (Y(I+1) - Y(I))^2)^{.5} + LEN(I)$

C CALCULATE SIN AND COS ANGLE OF INDIVIDUAL FRUSTUM

C-----  
 DO 102 I=1,N1  
 $SINB(I) = (Y(I+1) - Y(I)) / (LEN(I+1) - LEN(I))$   
 102  $COSB(I) = (X(I+1) - X(I)) / (LEN(I+1) - LEN(I))$

C FORMATION OF THE N BY N MATRIX

C-----  
 DO 103 I=1,N1  
 $XP = XM(I)$   
 $YP = YM(I)$   
 $SBP = SINB(I)$   
 $CBP = COSB(I)$   
 DO 103 J=1,N1  
 $XI = X(J)$   
 $XF = X(J+1)$   
 $YI = Y(J)$   
 $YF = Y(J+1)$   
 $XMP = XM(J)$   
 $YMP = YM(J)$   
 $LENI = LEN(J)$   
 $LENF = LEN(J+1)$   
 $SB = SINB(J)$   
 $CB = COSB(J)$   
 $CALL SELECT(XP, YP, XI, XF, YI, YF, LENI, LENF, M, LS)$   
 $IF (I.EQ.J) GO TO 50$   
 $CALL IEQJ(XP, YP, XI, XF, YI, YF, XMP, YMP, LENI, LENF,$   
 $SB, CB, SBP, CBP, M, I, J, XV, YV, VN, N1)$   
 GO TO 103  
 50  $CALL IEQJ(XP, YP, XI, XF, YI, YF, XMP, YMP, LENI, LENF,$   
 $SB, CB, SBP, CBP, M, I, J, XV, YV, VN, N1, IFACT)$   
 103 CONTINUE  
 DO 121 I=1,N1  
 DO 121 J=1,N1  
 121  $VN1(I, J) = VN(I, J)$

C TO FORM THE BOUNDARY CONDITION AT THE MID-POINT  
C OF EACH FRUSTUM

DO 104 I=1,N1  
104 VF(I)=0.0  
DO 105 J=1,NS  
105 VF(J)=UINF

C TO SOLVE FOR THE SURFACE DENSITY

CALL LEQT1F(VN,1,N1,N1,VF,0,C,IER)  
WRITE(6,7)(VF(I),I=1,N1)

C TO SOLVE THE VELOCITY AT ANY POINT  
C (THIS PORTION OF THE PROGRAM IS PERFORMED ONLY IF  
C ICT(3)=3)

IF(ICT(3).NE.3) GOTO 999  
WRITE(6,11)  
WRITE(6,17)

READ(5,1)NP  
DO 110 I=1,NP  
READ(5,9)PX,PY  
XVEF=0.0  
YVEF=0.0  
DO 112 J=1,N1  
XI=X(J)  
XF=X(J+1)  
YI=Y(J)  
YF=Y(J+1)  
SIGMA=VF(J)  
LENI=LEN(J)  
LENF=LEN(J+1)  
SB=SINB(J)  
CB=COSEB(J)

IF(PY.EQ.0.0)GO TO 111  
CALL YNEQO(PX,PY,XI,XF,YI,YF,SIGMA,LENI,LENF,  
SB,CB,XVE,YVE,LS)

GO TO 113

111 CALL YEQO(PX,PY,XI,XF,YI,YF,SIGMA,LENI,LENF,  
SB,CB,XVE,YVE,LS)

113 XVEF=XVE+XVEF

112 YVEF=YVE+YVEF

WRITE(6,7)XVEF,YVEF

110 CONTINUE

999 CONTINUE



C FORMAT STATEMENT  
C-----

```
1 FORMAT (I5)
2 FORMAT (6F10.5)
3 FORMAT (10E8.1)
4 FORMAT(F10.5)
5 FORMAT(10I5)
6 FORMAT(2I5,6E12.5)
7 FORMAT(10F10.6)
8 FORMAT(10F10.6)
9 FORMAT(2E10.5)
11 FORMAT(/)
17 FORMAT(7X,'X-VEL',10X,'Y-
STOP
END
```

```

C *****
C PROGRAM : MAIN
C PROGRAM TO CALCULATE THE TRAJECTORY AND
C TEMPERATURE OF THE DROPLET
C *****

```

```

C LIST OF VARIABLES :-

```

```

C CDRE -COEFFICIENT OF DRAG
C CHT -CONVECTIVE HEAT TRANSFER
C COSB -COSINE ANGLE OF THE FRUSTUM MADE WITH
C HORIZONTAL
C CP -SPECIFIC HEAT CAPACITY OF AIR
C CPWC -SPECIFIC HEAT CAPACITY OF AIR
C CW -SPECIFIC HEAT CAPACITY OF WATER
C DELT -TIME STEP FOR THE INTEGRATION OF THE EQUATION
C OF MOTION AND HEAT TRANSFER RATE
C DIA -DIAMETER OF THE DROPLET
C DIFF -DIFFUSIVITY OF WATER VAPOUR
C DTBDT -RATE OF CHANGE OF TEMPERATURE
C EMI -EMISSIVITY OF DROPLET (FOR RADIATIVE HEAT
C TRANSFER
C HDET -VARIABLE FOR DETERMINING THE VALUE OF NUSSELT
C NUMBER
C KA -THERMAL CONDUCTIVITY OF DRY AIR
C KF -THERMAL CONDUCTIVITY OF WATER VAPOUR
C KV -THERMAL CONDUCTIVITY OF AIR
C IC -COUNT INTEGER, IF IC IS EQUAL TO ICT(5) THE
C RESULT WILL BE PRINTED
C IC1 -COUNT INTEGER. IF IC1 IS EQUAL TO ICT(4) THE
C LOCATION OF THE DROPLET WILL BE CHECKED
C ICT(I)-CONTROL INTEGERS
C ICT(1) IF ICT(1) IS EQUAL TO '1' ALL THE INPUT
C CONDITION FOR THE TEST WILL BE PRINTED.
C NOTHING WILL BE PRINTED IF ICT(1) IS NOT
C EQUAL TO '1'.
C ICT(2) NOT USED
C ICT(3) NOT USED
C ICT(4) THE LOCATION OF THE DROPLET WILL BE
C CHECKED EVERY 'ICT(4)' TIME STEP. IF
C THE DROPLET IS OUTSIDE THE WIND TUNNEL
C A WARNING MESSAGE WILL BE PRINTED
C ICT(5) THE RESULT OF THE EVERY 'ICT(5)' TIME
C STEP WILL BE PRINTED. (TIME SAVING DEVICE)
C IOU -CONTROL VARIABLE. IF IOU IS EQUAL TO '2', THE
C DROPLET IS OUTSIDE THE TUNNEL, A WARNING
C MESSAGE WILL BE PRINTED.

```

```

C -- CONTINUE --
C -----

```

```

C-----*
C LIST OF VARIABLES :-*
C IFAT -CONTROL VARIABLE. A FLAG TO CHANGE THE UPPER*
C AND LOWER PERCENTAGE CHANGE ON VELOCITY IF THE*
C DROPLET IS BEYOND THE LIMIT 'LIMITU'. RESULTS*
C WILL BE PRINTED EVERY TIME STEP AFTER 'LIMITU'.*
C LC -LOWER CONTROL LIMIT FOR THE PERCENTAGE CHANGE*
C IN DROPLET VELOCITY (FOR TIME STEP CALCULATION)*
C LEN -ACCUMULATED LENGTH OF THE WIND TUNNEL*
C LIMITL-LOCATION WHERE THE VALUES OF THE DROPLET*
C PROPERTIES IS REQUIRED. AT THIS POINT THE*
C PROGRAM WILL STOP*
C LIMITU-UPPER LIMIT FOR THE X-CO-ORDINATE AT THE WIND*
C TUNNEL. AT THIS LOCATION THE UC AND LC VALUE*
C WILL CHANGE TO A SMALLER VALUE. THIS IS TO MAKE*
C SURE THE DROPLET PASS THROUGH THE REGION*
C BETWEEN LIMITU AND LIMITL IN A SMALLER TIME*
C INCREMENT*
C LV -LATENT HEAT OF VAPORIZATION OF WATER*
C MDET -VARIABLE FOR DETERMINING THE VALUE OF SHERWOOD*
C NUMBER*
C MHT -MASS HEAT TRANSFER*
C NU -NUSELT NUMBER*
C PA -PRESURE OF AIR INSIDE THE TUNNEL*
C PAW -SATURATED WATER VAPOUR PRESSURE*
C PD -VAPOUR PRESSURE OF THE DROPLET*
C PF -FILM VAPOUR PRESSURE ON THE SURFACE OF THE*
C DROPLET*
C PR -PRANDTH NUMBER*
C RA -GAS CONSTANT (IDEAL GAS LAW)*
C RATIO -VELOCITY RATIO*
C RE -REYNOLDS NUMBER*
C RH -RELATIVE HUMIDITY OF AIR (0.0 TO 1.0)*
C RHOA -DENSITY OF AIR*
C RHOD -DENSITY OF WATER DROPLET*
C RHT -RADIATIVE HEAT TRANSFER*
C RV -WATER VAPOUR CONSTANT*
C SC -SMITH NUMBER*
C SH -SHERWOOD NUMBER*
C SIG -STEFAN BLTOZMANN CONSTANT*
C SINB -SINE ANGLE OF THE FRUSTUM MADE WITH THE*
C HORIZONTAL*
C T -ACCUMULATED TIME THAT THE DROPLET SPEND IN THE*
C TUNNEL*
C TA -TEMPERATURE OF AIR*
C TD -TEMPERATURE OF DROPLET*
C TF -FILM TEMPERATURE ON THE SURFACE OF THE DROPLET*
C
C -- CONTINUE --
C-----*

```

```

C-----*
C
C LIST OF VARIABLES :-
C UC      -UPPER CONTROL LIMIT FOR PERCENTAGE CHANGE IN
C          DROPLET VELOCITY (FOR TIME STEP CALCULATION)
C VA,UA,WA-VELOCITY COMPONENTS OF AIR IN X, Y AND Z
C          DIRECTION
C VD,UD,WD-VELOCITY COMPONENTS OF DROPLET IN X, Y AND Z
C          DIRECTION
C VELA    -RESULTANT VELOCITY OF AIR
C VELD    -RESULTANT VELOCITY OF WATER DROPLET
C VF(I)   -ARRAY OF SOURCE DENSITY
C VIS     -DYNAMIC VISCOSITY OF AIR
C X(I)    -X CO-ORDINATE OF THE WIND TUNNEL
C XL,YL,ZL-CO-ORDINATE OF DROPLET IN X, Y AND Z DIRECTION
C XM(I)   -MID POINT OF EACH FRUSTUM (X CO-ORDINATE)
C Y(I)    -Y CO-ORDINATE OF THE WIND TUNNEL
C YM(I)   -MID POINT OF EACH FRUSTUM (Y CO-ORDINATE)
C
C*****

```

```

REAL X(130),Y(130),LEN(130),XM(129),YM(129),
@ X1,Y1,XF,YF,XMP,YMP,VF(129),VN(129,129),
@ X2,Y2,XV,YV,VN1(129,129),
@ SINB(129),COSB(129),C(129),VT(129),NV(129),...
@ X(300),Y(300)
@ XE,YE,LO,UA,VA,WA,UD,VD,WD,CDRE,DTBDT
@ PX,PY,XVEF,YVEF,LIMITL,LIMITU,SBP,CBP,
@ TF,DFE,LV,PD,PF,KA,KV,KF,SC,PR,MDET,HDET,
@ RHT,MHT,CHT,PV,UCRT,LCRT,CONS,LCVT,UCVT,
@ LENI,LENF,RATIO,DUBDT,DVBDT,DWBDT,CRT,UC,LC
@ DTBDT,CONS,UC,LC,LCVT,UCVT,CRT,
DIMENSION ICT(5)

```

```

C REAL IN INPUT DATA
C-----

```

```

READ (5,5) (ICT(I),I=1,5)
WRITE (6,5) (ICT(I),I=1,5)
READ(5,4)RATIO
READ (5,1) N
READ (5,2)(X(I),I=1,N)
READ (5,2)(Y(I),I=1,N)
LS=16
N1=N-1
READ (5,8)(VF(I),I=1,N1)
DO 99 I=1,N1
99 VF(I)=VF(I)*RATIO

```

C CALCULATE THE MID-POINT OF EACH FRUSTUM(TOTAL OF N-1)  
C-----

DO 100 I=1,N1  
XM(I)=(X(I)+X(I+1))/2.0  
100 YM(I)=(Y(I)+Y(I+1))/2.0

C CALCULATE THE ACCUMULATED LENGTH OF THE TUNNEL  
C AT EACH FRUSTUM  
C-----

LEN(1)=0.0  
DO 101 I=1,N1  
101 LEN(I+1)=((X(I+1)-X(I))\*\*2+(Y(I+1)-Y(I))\*\*2)\*\*.5+  
1LEN(I)

C CALCULATE SINE AND COSINE ANGLE OF EACH FRUSTUM  
C-----

DO 102 I=1,N1  
SINB(I)=(Y(I+1)-Y(I))/(LEN(I+1)-LEN(I))  
102 COSB(I)=(X(I+1)-X(I))/(LEN(I+1)-LEN(I))

C READ IN INITIAL PROPERTIES OF THE DROPLET.  
C SPECIFY THE UPPER AND LOWER LOCATION AT THE TUNNEL  
C AND UPPER AND LOWER PERCENTAGE CHANGE IN VELOCITY  
C-----

READ (5,8) XL,YL,ZL,LIMITU,LIMITL  
READ (5,8) UC,LC  
READ (5,2) UD,VD,WD,DELT

C READ IN THE DIAMETER OF THE DROPLET, INITIAL  
C TEMPERATURE OF DROPLET AND AIR, AND THE RELATIVE  
C HUMIDTY OF AIR  
C-----

READ (5,2) DIA,TD,TA,RH  
READ (5,2) VIS,RHOD,RHOA

C SPECIFY THE THE VALUES OF CONSTANTS  
C-----

RA=287.05  
RV=461.51  
EMI=0.95  
C1=2\*3.14159\*DIA  
C2=RHOA\*TA  
SIG=5.6687D-08  
CON=48.\*VIS/(DIA\*DIA\*RHOD)  
CPHC=1800.0  
CP=1005.  
PA=C2\*RA  
PAW=VAP(TA)\*RH  
IC=1  
IC1=1  
IOU=1  
IFAT=0  
T=0.0

C OUTPUT THE INITIAL CONDITION OF THE DROPLET AND  
C THE SPECIFIED CONDITION OF THE TEST. FOR THESE TO  
C BE PRINTED OUT ICT(1) MUST BE EQUAL TO '1'  
C-----

IF (ICT(1) .NE. 1) GOTO 53  
CPHC=1800.0  
WRITE(6,18) XL,YL,ZL,UD,VD,WD,DELT  
WRITE(6,19) DIA  
WRITE(6,20) TA,TD,RH  
WRITE(6,21) VIS,RHOA,RHOD  
53 WRITE(6,22)

C CALCULATE THE AIR VELOCITY AT POINT XL,YL,ZL,  
C AND THE RESULTANT VELOCITY OF AIR AND DROPLET  
C-----

CALL VEL(XL,YL,ZL,VF,X,Y,LEN,SINB,COSB,N,N1,LS,UA,VA,WA)  
VELA=(UA\*UA+VA\*VA+WA\*WA)\*\*0.5  
VELD=(UD\*UD+VD\*VD+WD\*WD)\*\*0.5

C TEST THE POSITION OF THE DROPLET. IF XL IS GREATER  
C 'LIMITU', ICT(5) WILL BE CHANGED TO '1' AND RESULTS  
C WILL BE PRINTED EVERY TIME STEP  
C-----

52 CONTINUE  
IF(XL .GT. LIMITU) ICT(5)=1

C RESET COUNTER

C-----

IF(ICT(5) .EQ. 1) IC=1

C TEST THE COUNTER 'IC1' TO FIND OUT IF THE LOCATION  
C OF THE DROPLET REQUIRED TO BE CHECKED

C-----

IF(IC1 .EQ. ICT(4)) GOTO 70

GOTO 71

70 CALL TEST(XL,YL,ZL,X,Y,N1,IOU)

IF(IOU .EQ. 2) GOTO 999

IC1=1

C CALCULATE THE VELOCITY DIFFERENCE BETWEEN THE DROPLET  
C AND AIR, TO ENSURE THAT THE DIFFERENCE IS NOT SMALLER  
C THAN 0.005 M/S

C-----

71 DUD=ABS(UA-UD)

DVD=ABS(VA-VD)

DWD=ABS(WA-WD)

IF(DUD .LT. 0.005) UD=UA

IF(DVD .LT. 0.005) VD=VA

IF(DWD .LT. 0.005) WD=WA

C TO CALCULATE THE REYNOLDS NUMBER AND THE  
C COEFFICIENT OF DRAG

C-----

VEL1=VELA

RE=DIA\*RHOA\*ABS(VELA-VELD)/VIS

IF(RE .LT. 0.2) CDRE=1.

IF(RE .GE. 0.2 .AND. RE .LT. 2.0) CDRE=1.0+0.102\*RE\*\*0.955

IF(RE .GE. 2.0 .AND. RE .LT. 21.0) CDRE=1.0+0.115\*RE\*0.802

IF(RE .GE. 21.0 .AND. RE .LT. 200.0) CDRE=1.0+0.189\*RE\*\*0.632

IF(RE .GE. 200.0) GOTO 888

C CALCULATE THE RATE OF CHANGE OF VELOCITY FOR  
C EACH COMPONENTS

C-----

DUBDT=CDRE\*CON\*(UA-UD)

DVBDT=CDRE\*CON\*(VA-VD)-9.81

DWBDT=CDRE\*CON\*(WA-WD)

C. TO REGULATE THE TIME INTERVAL FOR INTEGRATION

C-----

```

IF(ABS(DUBDT).LT.0.5 .AND. ABS(DVBDT).LT.10.0) GOTO 58
IF(XL .GT. LIMITU .AND. IFAT .EQ. 0) GOTO 56
GOTO 57
56 UC=UC/5.0
   LC=LC/5.0
   IFAT=1
57 IF(ABS(UD).LT.0.05 .OR. ABS(DUBDT).LT.1.0) GOTO 55
   CRT=ABS(UD/DUBDT)
   UCRT=UC*CRT
   LCRT=LC*CRT

```

```

IF(DELT .GT. UCRT) DELT=UCRT
IF(DELT .LT. LCRT) DELT=LCRT

```

```

55 IF (ABS(VD).LT. 0.05 .OR. ABS(DVBDT).LT.0.5) GOTO 59
   CVT=ABS(VD/DVBDT)
   UCVT=UC*CVT
   LCVT=LC*CVT
   IF(LCVT .LT. LCRT) LCRT=LCVT
   IF(UCVT .LT. UCRT) UCRT=UCVT

```

```

IF(DELT .GT. UCRT) DELT=UCRT
IF(DELT .LT. LCRT) DELT=LCRT
GOTO 59

```

```

58 DELT=DELT*1.05

```

C INTERGATE THE RATE OF CHANGE OF VELOCITY OF THE  
C PROPLET TO OBTAIN THE VELOCITIES AND POISTIONS

C-----

```

59 DELU=DUBDT*DELT
   DELX=(UD+DUBDT*DELT/2.)*DELT
   UD=UD+DELU
   XL=XL+DELX

```

```

   DELV=DVBDT*DELT
   DELY=(VD+DVBDT*DELT/2.)*DELT
   VD=VD+DELV
   YL=YL+DELY

```

```

   DELW=DWBDT*DELT
   DELZ=(WD+DWBDT*DELT/2.)*DELT
   WD=WD+DELW
   ZL=ZL+DELZ

```



C CALCULATE THE AIR VELOCITY FOR THE NEW POSITION  
C AND THE RESULTANTS OF AIR AND DROPLET  
C-----

CALL VEL(XL,YL,ZL,VF,X,Y,LEN,SINB,COSB,N,N1,LS,UA,VA,WA)  
VELA=(UA\*UA+VA\*VA+WA\*WA)\*\*0.5  
VELD=(UD\*UD+VD\*VD+WD\*WD)\*\*0.5

C CALCULATE THE CHANGE IN AIR TEMPERATURE DUE TO THE  
C CONTRACTION OF THE WIND TUNNEL  
C-----

TA1=TA-(VELA\*\*2-VEL1\*\*2)/CPHC  
PAW=PAW\*ABS(TA1/TA)\*\*1.4  
TA=TA1  
RHOA=C2/TA

C CALCULATE THE THERMAL CONDUCTIVITY OF AIR  
C-----

TF=(TA+TD)/2.  
DFF=0.211/10\*\*4\*(101325./PA)\*(TF/273.15)\*\*1.94  
LV=2.501\*10\*\*6-2340.8\*(TD-273.15)  
PD=VAP(TD)  
PF=(PAW+PD)/2.  
KA=4.1868/10\*\*3\*(5.69+.017\*(TF-273.15))  
KV=4.1868/10\*\*3\*(3.78+.020\*(TF-273.15))  
KF=KA\*(1-(1.17-1.02\*KV/KA)\*PAW/(PA+PAW))

C CALCULATE THE SCDMIDCT NUMBER, NUSSELT NUMBER,  
C SHERWOOD NUMBER AND NUSSELT NUMBER  
C-----

SC=VIS/(RHOA\*DFF)  
PR=CP\*VIS/KF  
MDET=SC\*\*(1./3.)\*RE\*\*0.5  
HDET=PR\*\*(1./3.)\*RE\*\*0.5  
IF(MDET.LT.0.4) SH=1.+0.108\*MDET\*\*2  
IF(MDET.GE.0.4) SH=0.78+.308\*MDET  
IF(HDET.LT.1.4) NU=1.+0.108\*HDET\*\*2  
IF(HDET.GE.1.4) NU=0.78+.308\*HDET

C CALCULATE THE THREE FORMS OF HEAT TRANSFERS  
C-----

MHT=C1/RV\*LV\*DFF\*(PAW/TA-PD/TD)\*SH/2  
PV=PAW/PA  
CHT=C1\*KF\*(TA-TD)\*NU/2  
RHT=C1\*SIG\*EMI\*DIA/2\*(TA\*\*4-TD\*\*4)

C CALCULATE THE SPECIFIC HEAT CAPACITY OF WATER,  
 C AND THE CHANGE IN INTERNAL ENERGY OF THE DROPLET  
 C-----

```

    IF(TD.GT.273.15) CW=4186.84*(.9979+3.1/10**6
    @*(TD-308.15)**2
    1+3.8/10**9*(TD-308.15)**4
    IF(TD.LE.273.15) CW=4186.84*(1.0074+8.29/10**5
    @*(TD-273.15)**2
    CONS=C1*DIA**2/12.*RHOD*CW
    DTBDT=(MHT+CHT+RHT)/CONS
    DT=DTBDT*DELT
  
```

```

    TD=TD+DT
    T=T+DELT
  
```

C INCREMENT THE COUNTERS AND CHECK IF OUTPUT IS REQUIRED  
 C-----

```

    IC1=IC1+1
    IF(IC.EQ. ICT(5)) GOTO 60
    IC=IC+1
    GOTO 61
  60 WRITE(6,7) T,XL,YL,ZL,DUBDT,DVBDT,DWBDT,UD,VD,WD,
    @UA,VA,WA,TD,TA
    1DELT
    IC=1
  61 CONTINUE

    IF(XL.GT. LIMITL) GOTO 51
    GOTO 52
  888 WRITE(6,9)
    GOTO 51
  999 WRITE(6,12)
    51 CONTINUE
  
```

C FORMAT STATEMENTS  
 C-----

```

    1 FORMAT (I5)
    2 FORMAT (6E10.5)
    3 FORMAT (10E8.1)
    4 FORMAT(F10.5)
    5 FORMAT(10I5)
    6 FORMAT(2I5,6E12.5)
    7 FORMAT(13F8.4,2F8.3,F8.5)
    8 FORMAT(10F10.6)
    9 FORMAT(7X,'RE IS LARGER THAN 200.0!')
   10 FORMAT(6F10.6)
   11 FORMAT(/)
  
```

```

12 FORMAT(10X,'THE DROPLET IS OUTSIDE THE WIND TUNNEL!')
13 FORMAT(20X,'THE SOURCE DENSITY')
14 FORMAT(20X,'THE TANGENTIAL VELOCITY')
15 FORMAT(20X,'THE NORMAL VELOCITY')
16 FORMAT(20X,'THE BACK SUBSTITUTION')
17 FORMAT(7X,'X-VEL',10X,'Y-VEL')
18 FORMAT(5X,'INITIAL POSITION OF THE DROPLET',2X,
@'X0=',F10.5,/,38X,'Y0=',F10.5,/,38X,'Z0=',F10.5,/,
@5X,'INITIAL VELOCITY OF THE DROPLET',2X,'UD=',F10.5,
@/,38X,'VD=',F10.5,/,38X,'WD=',F10.5,/,
@5X,'INITIAL TIME STEP' DELT=',F10.5,/)
19 FORMAT(5X,'DIAMETER OF THE DROPLET' DIA=',F11.6)
20 FORMAT(5X,'INITIAL TEMPERATURE OF AIR' TA=',F10.5,
@'(K)',/,5X,'INITIAL TEMPERATURE OF DROPLET' TD=',F10.5,
@'(K)',/,5X,'RELATIVE HUMIDITY OF AIR' RH=',F10.5
21 FORMAT(5X,'VISCOSITY OF AIR' VIS=',F11.6
@/,5X,'DENSITY OF AIR' RHOA=',F10.5,/,
@5X,'DENSITY OF DROPLET' RHOD=',F10.5,/)
22 FORMAT(7X,'T',6X,'XL',6X,'YL',6X,'ZL',3X,'DUBDT',
@3X,'DVBDT',3X,'DWBDT',5X,'UD',6X,'VD',6X,'WD',
@6X,'UA',6X,'VA',6X,'WA',6X,'TD',6X,'TA')
STOP
END

```

```

C*****
C
C SUBROUTINE: INEQJ
C          -CALCULATION OF SURFACE INTEGRAL FOR
C          FRUSTUM I IS NOT EQUAL TO FRUSTUM J.
C*****
C
C LIST OF VARIABLES:-
C H          -WIDTH OF SUBELEMENT
C HL         -INCREMENT LENGTH ALONG THE TUNNEL SURFACE
C LEND       -WIDTH OF ELEMENT
C XE,YE      -X AND Y CO-ORDINATE OF THE SUBELEMENT
C EI         -ARGUMENT OF ELLIPTICAL INTEGRAL
C EK         -ELLIPTICAL INTEGRAL OF THE 1st KIND
C KK         -ELLIPTICAL INTEGRAL OF THE 2nd KIND
C IER        -IF EI=1.0 EK & KK DO NOT EXIST
C            -IF EI=1.0 EK & KK WILL BE CALCULATED BY
C            SUBROUTINE
C FX(I)      -INTEGRAL VALUE FOR SIMPSON'S RULE CALCULATION
C FY(I)      -INTEGRAL VALVE FOR SIMPSON'S RULE CALCULATION
C XV(I,J)    -X VELOCITY POTENTIAL FOR FRUSTUM I DUE TO
C            FRUSTUM J
C YV(I,J)    -Y VELOCITY POTENTIAL FOR FRUSTUM I DUE TO
C            FRUSTUM J
C VN(I,J)    -VELOCITY POTENTIAL NORMAL TO THE SURFACE
C            FOR FRUSTUM I DUE TO FRUSTUM J
C*****
C
C SUBROUTINE INEQJ(XP,XP,XI,XF,YI,YF,XMP,YMP,XV,YV,VN,
@      LENI,LENF,SB,CB,SBP,CBP,M,IC,JC,N)
C REAL XP,YP,XI,XF,YI,YF,LENI,LENF,SB,CB,H,HL,XE,YE,
@      KK,EK,EI,YV(N,N),LEND,
@      FX(300),FY(300),VN(N,N),XV(N,N),YV(N,N)
C
C TO INITIALIZE THE ARRAYS
C-----
C
C DO 12 I=1,300
C   FX(I)=0.0
C   FY(I)=0.0
C 12 CONTINUE
C   M1=M+1
C   M2=M-1
C
C TO CALCULATE THE INTERVAL
C-----
C
C H=(XF-XI)/M
C HL=(LENF-LENI)/M

```

C TO CALCULATE THE (EPSCLON) AND (ETA) FOR EACH  
C SUBELEMENT OF THE ELLIPTICAL INTEGRALS

```

C-----
      LEND=LENF-LENI
      DO 10 I=1,M1
      XE=XI+((I-1)*HL)*CB
      YE=YI+((I-1)*HL)*SB
      EI=4*YP*YE/((YP+YE)**2+(XP-XE)**2)
      IER=0
      CALL ELIP(EI,EK,KK,IER)
      IF(IER.EQ. 1) GOTO 13

```

C TO CALCULATE THE SURFACE INTEGRAL

```

C-----
      FX(I)=-4*YE*(XP-XE)*EK/((((YP+YE)**2+(XP-XE)**2)**.5)
      @*((YP-YE)**2+(XP-XE)**2))
      FY(I)=((-2*YE)/(YP*((YP+YE)**2+(XP-XE)**2)**0.5))
      @*(KK+((YP*YE**2-(XP-XE)**2)/((YP-YE)**2+(XP-XE)
      @**2))*EK)
10  CONTINUE
      XV(IC,JC)=0.0
      YV(IC,JC)=0.0
      DO 11 I=1,M2,2
      XV(IC,JC)=(FX(I)+4*FX(I+1)+FX(I+2))*HL/3+XV(IC,JC)
      YV(IC,JC)=(FY(I)+4*FY(I+1)+FY(I+2))*HL/3+YV(IC,JC)
11  CONTINUE
      VN(IC,JC)=XV(IC,JC)*(-SBP)+YV(IC,JC)*CBP
13  RETURN
      END

```

```

C*****
C
C SUBROUTINE : IEQJ
C          CALCULATION OF SURFACE INTEGRAL FOR
C FRUSTUM I IS EQUAL TO FRUSTUM J
C
C-----
C FRUSTUM I IS DIVIDED INTO THREE REGIONS. THE FIRST-
C AND THIRD REGIONS ARE INTEGRATED BY SIMPSON'S
C RULE METHOD. WHILE THE CENTRE REGION IS INTEGRATED
C BY POWER FUNCTION.
C*****
C
C LIST OF VARIABLES:- (SEE ALSO INEQJ)
C SM      -CONSTANT FOR THE WIDTH OF THE CENTRE SECTION
C SS      -THE WIDTH OF THE CENTRE SECTION
C XV1     -X VELOCITY POTENTIAL DUE TO THE CENTRE SECTION
C YV1     -Y VELOCITY POTENTIAL DUE TO THE CENTRE SECTION
C XF1     -FINAL X CO-ORDINATE OF THE FIRST REGION
C YF1     -FINAL Y CO-ORDINATE OF THE FIRST REGION
C VN(I,J) -NORMAL VELOCITY COMPONENT
C
C*****

```

```

SUBROUTINE IEQJ(XP,YP,XI,XF,YI,YF,XMP,YMP,LENI,LENF,
@ SB,CB,SBP,CBP,M,IC,JC,XV,YV,VN,N,IFACT)
REAL XI,XF,YI,YF,LENI,LENF,SB,CB,XV(N,N),YV(N,N),
@ VN(N,N),LENF1,LENI2,XP,YP,SBP,CBP

```

```

C INTEGRATION OF THE CENTRE REGION
C-----

```

```

SM=0.01
SS=YP*SM
XV1=SB*CB*(2*SM+(13/72+1/12*ALOG(SM/8)+1/12*SB**2)
@ *SM**3)
YV1=(2*SB**2+2*ALOG(SM/8))*SM-((3+3*ALOG(SM/8)
@ -3*SB**2-2*SB**4)*SM**3)/24

```

```

C INTEGRATION OF THE FIRST REGION
C-----

```

```

LENF1=(LENF+LENI)/2-SS
XF1=XP-SS*CB
YF1=YP-SS*SB
CALL INEQJ(XP,YP,XI,XF1,YI,YF1,XMP,YMP,LENI,LENF1,
@ SB,CB,SBP,CBP,M,IC,JC,XV,YV,VN,N)
XXV=XV(IC,JC)
YYV=YV(IC,JC)
VN2=VN(IC,JC)

```

C INTEGRATION OF THE THIRD REGION

C-----

```

      LENI2=(LENF+LENI)/2+SS
      XI2=XP+SS*CB
      YI2=YP+SS*SB
      CALL INEQJ(XP,YP,XI2,XF,YI2,YF,XMP,YMP,LENI2,LENF,
      @SB,CB,SBP,CBP,M,IC,JC,XV,YV,VN,N)
      PY=2.*3.141593
      IF IFACT.NE. 1) PY=-PY
      XV(IC,JC)=XV(IC,JC)+XXV-PY*SB+XV1
      YV(IC,JC)=YV(IC,JC)+YYV+PY*CB+YV1
      VN3=VN(IC,JC)
      VN(IC,JC)=0.0

```

C SUMMATION OF THE THREE REGIONS

C-----

```

      VN(IC,JC)=-XV1*SBP+YV1*CBP+VN2+VN3+PY
      RETURN
      END

```

```

C*****
C
C SUBROUTINE : YNEQO
C -CALCULATION OF THE VELOCITY COMPONENTS
C AT A LOCATION WHEN Y CO-ORDINATE IS NOT EQUAL TO ZERO
C*****
C LIST OF VARIABLES:-
C FX,FY -VALUES OF INTEGRATION AT EACH SUBELEMENT
C XV,YV -VELOCITY COMPONENTS AT THE REQUIRED POINT
C*****
C SUBROUTINE YNEQO(XP,YP,XI,XF,YI,YF,SIG,LENI,LENF,
C SB,CB,XV,YV,LS)
C REAL XP,YP,XE,YE,SIG,LENI,LENF,SB,CB,XV,YV,LEND
C REAL EI,EK,KK,FX(91),FY(91)

C INITIALIZE THE ARRAYS AND CALCULATE THE NUMBER OF
C SUB-ELEMENTS ON THE FRUSTUM
C-----

DO 10 I=1,91
  FX(I)=0.0
10 FY(I)=0.0
  CALL SELECT(XP,YP,XI,XF,YI,YF,LENI,LENF,M,LS)
  M1=M+1
  M2=M-1

C CALCULATE THE WIDTH OF THE SUB-ELEMENT
C-----

H=(XF-XI)/M
HL=(LENF-LENI)/M
LEND=LENF-LENI

C CALCULATE THE INFLUENCE DUE TO EACH SUB-ELEMENT
C-----

DO 11 I=1,M1
  XE=XI+(I-1)*HL*CB
  YE=YI+(I-1)*HL*SB
  EI=ABS(4*YP*YE/((YP+YE)**2+(XP-XE)**2))
  IER=0
  CALL ELIP(EI,EK,KK,IER)
  IF(IER.EQ. 1) GOTO 13
  FX(I)=-4*YE*(XP-XE)*EK/(((YP+YE)**2+(XP-XE)**2)
  @**0.5)*((YP-YE)**2+(XP-XE)**2))*SIG
  FY(I)=((-2*YE)/(YP*((YP+YE)**2+(XP-XE)**2)**0.5))
  @*(KK+((YP**2-YE**2-(XP-XE)**2)/((YP-YE)**2+(XP-XE)
  @**2))*EK)*SIG
11 CONTINUE

```



C SUMMATION USING SIMPSON'S RULE  
C-----

```
XV=0.0
YV=0.0
DO 12 I=1,M2,2
  XV=(FX(I)+4*FX(I+1)+FX(I+2))*HL/3+XV
  YV=(FY(I)+4*FY(I+1)+FY(I+2))*HL/3+YV
-- 12
13 RETURN
END
```



```

C*****
C
C SUBROUTINE : YEQO
C           - CALCULATION OF THE VELOCITY COMPONENTS
C AT A LOCATION WHEN THE Y CO-ORDINATE IS EQUAL TO ZERO
C*****
C
C LIST OF VARIABLES :-
C FX      -VALUE OF INTEGRATION AT EACH SUBELEMENT
C XV,YV   -VELOCITY COMPONENTS AT THE REQUIRED POINT
C*****
C
C SUBROUTINE YEQO(XP,YP,XI,XF,YI,YF,SIG,LENI,LENF,
C SB,CB,XV,YV,LS)
C REAL XP,YP,XE,YE,SIG,LENI,LENF,SB,CB,XV,YV,
C FX(91),LEND
C
C CALCULATE THE NUMBER OF SUB-ELEMENT ON THE FRUSTUM
C AND THE WIDTH OF EACH FRUSTUM
C-----
C
C CALL SELECT(XP,YP,XI,XF,YI,YF,LENI,LENF,M,LS)
C M1=M+1
C M2=M-1
C H=(XF-XI)/M
C HL=(LENF-LENI)/M
C
C CALCULATE THE INFLUENCE DUE TO THE SUB-ELEMENTS
C-----
C
C LEND=LENF-LENI
C EK=1.5708
C DO 10 I=1,M1
C   XE=XI+(I-1)*HL*CB
C   YE=YI+(I-1)*HL*SB
C   FX(I)=-4*YE*(XP-XE)*EK/((((YP+YE)**2+(XP-XE)**2)
C @**.5)*((YP-YE)**2+(XP-XE)**2))*SIG
C 10 CONTINUE
C
C SUMMATION USING SIMPSON'S RULE
C-----
C
C XV=0.0
C YV=0.0
C DO 12 I=1,M2,2
C 12 XV=(FX(I)+4*FX(I+1)+FX(I+2))*HL/3+XV
C RETURN
C END

```

```

C*****
C
C SUBROUTINE :SELECT
C           -CALCULATION OF THE NUMBER OF
C SUB-ELEMENT FOR NUMERICAL INTEGRATION
C
C*****
C
C LIST OF VARIABLES:-
C XI,YI -INITIAL X, Y CO-ORDINATE OF THE FRUSTUM
C XF,YF -FINAL X, Y CO-ORDINATE OF THE FRUSTUM
C LEND -THE TOTAL LENGTH OF THE FRUSTUM
C M -TOTAL NUMBER OF SUBELEMENT ON THE FRUSTUM
C LS -MINIMUM NUMBER OF SUB-ELEMENTS ON THE FRUSTUM
C D1 -DISTANCE FROM THE INITIAL POINT ON THE FRUSTUM
C     TO THE REQUIRED POINT
C D2 -DISTANCE FROM THE FINAL POINT ON THE FRUSTUM
C     TO THE REQUIRED POINT
C DMIN -THE LESSER VALUE OF D1 AND D2
C*****

```

```

SUBROUTINE SELECT (XP,YP,XI,XF,YI,YF,LENI,LENF,M,LS)
REAL *XP,YP,XI,XF,YI,YF,LENI,LENF,LEND

```

```

C CALCULATE THE MINIMUM DISTANCE FROM THE FRUSTUM TO
C THE REQUIRED POINT
C-----

```

```

D1=((XP-XI)**2+(YP-YI)**2)**.5
D2=((XP-XF)**2+(YP-YF)**2)**.5
DMIN=D2
IF(D1.LE.D2) DMIN=D1

```

```

C CALCULATE THE NUMBER OF SUB-ELEMENT (EVEN NUMBER)
C-----

```

```

LEND=LENF-LENI
N=IFIX(LS*LEND/DMIN)
IF (N.EQ.0) GO TO 11
K=N/2
L=K*2
M=N
IF (L.NE.N)M=N+1
GO TO 10
11 M=2
10 RETURN
END

```

```

C*****
C
C SUBROUTINE :VEL
C          -CALCULATION OF THE THREE VELOCITY
C COMPONENTS OF AIR AT THE REQUIRED LOCATIONS
C*****
C
C LIST OF VARIABLES:-
C XL      -X CO-ORDINATE
C YL      -Y CO-ORDINATE
C ZL      -Z CO-ORDINATE
C RL      -RADIAL LOCATION
C SIGMA   -SOURCE DENSITY
C UA      -VELOCITY COMPONENT IN THE X DIRECTION
C VA      -VELOCITY COMPONENT IN THE Y DIRECTION
C ZA      -VELOCITY COMPONENT IN THE Z DIRECTION
C*****

```

```

SUBROUTINE VEL (XL,YL,ZL,VF,X,Y,LEN,SINB,COSB,
@ N,N1,LS,UA,VA,WA)
REAL XL,YL,ZL,RL,X(N),Y(N),VF(N1),SINB(N1),COSB(N1),
@ LEN(N),XVE,XVEF,YVE,YVEF,UA,VA,WA,SIGMA,LENI,LENF,
@ SB,CB

```

```

C CALCULATE THE RADIUS OF THE TUNNEL AT LOCATION XL
C-----

```

```

RL=(YL*YL+ZL*ZL)**0.5
IF(RL .EQ. 0.0) GOTO 100
SIND=YL/RL
COSD=ZL/RL
GOTO 101
100 SIND=0.0
COSD=0.0

```

```

C CALCULATE THE VELOCITY POTENTIAL AT THE REQUIRED
C POINT DUE TO THE INFLUENCE OF EVERY FRUSTUM
C-----

```

```

101 XVEF=0.0
YVEF=0.0
DO 112 J=1,N1
XI=X(J)
XF=X(J+1)
YI=Y(J)
YF=Y(J+1)
SIGMA=VF(J)
LENI=LEN(J)
LENF=LEN(J+1)
SB=SINB(J)
CB=COSB(J)

```

C SELECT THE SUBROUTINE AND CALCULATE THE VELOCITY  
C COMPONENTS  
C-----

IF (RL .EQ. 0.0) GOTO 111  
CALL YNEQO(XL,RL,XI,XF,YI,YF,SIGMA,LENI,LENF,SB,CB,  
@XVE,YVE,LS)  
GOTO 113  
111 CALL YEQO(XL,RL,XI,XF,YI,YF,SIGMA,LENI,LENF,SB,CB,  
@XVE,YVE,LS)

C SUMMATION  
C-----

113 XVEF=XVEF+XVE  
YVEF=YVEF+YVE  
112 CONTINUE

C RESOLVE INTO THE THREE VELOCITY COMPONENTS  
C-----

UA=XVEF  
VA=YVEF\*SIND  
WA=YVEF\*COSD  
RETURN  
END

```

C*****
C
C FUNCTION : VAP
C          -CALCULATION OF THE WATER VAPOUR PRESSURE
C          AT TEMPERATURE T.
C*****
C
C LIST OF VARIABLES:-
C VAP  -WATER VAPOUR PRESSURE (UNIT IN PASCAL)
C T    -TEMPERATURE (KEVIN)
C*****

```

```

REAL FUNCTION VAP(T)
REAL A0,A1,A2,A3,A4,A5,A6,T
A0=6984.505294
A1=-188.9039310
A2=2.133357675
A3=-1.2885809730D-02
A4=4.393587233D-05
A5=-8.023923082D-08
A6=6.136820929D-11
VAP=(A0+T*(A1+T*(A2+T*(A3+T*(A4+T*(A5+T*(A6))))))*100.
RETURN
END

```

```

C*****
C
C SUBROUTINE :ELIP
C           - EVALUATION OF THE ELLIPTICAL INTEGRAL
C OF THE 1st AND 2nd KIND
C
C*****
C
C LIST OF VARIABLES :-
C EI      - ARGUMENT OF THE ELLIPTICAL INTEGRAL
C EK      - ELLIPTICAL INTEGRAL OF THE FIRST KIND
C KK      - ELLIPTICAL INTEGRAL OF THE SECOND KIND
C
C*****

```

```

SUBROUTINE ELIP(EI,EK,KK,IER)
REAL EI,EK,KK,ELN,ETA

```

```

ETA=1.-EI
IF(ETA.LE. 0.0) GOTO 10
ELN=ALOG(ETA)

```

```

C CALCULATE THE ELLIPTICAL INTEGRAL OF THE FIRST KIND
C-----

```

```

EK=1+ETA*(0.44325141463+ETA*(0.0626060122+ETA
@*(0.04757383546+ETA*0.01736506451)))-ELN*(ETA
@*(0.2499836831+ETA*(0.9200180037+ETA*(0.04069697526
@+ETA*0.00526449639))))

```

```

C CALCULATE THE ELLIPTICAL INTEGRAL OF THE SECOND KIND
C-----

```

```

KK=1.38629436112+ETA*(0.09666344259+ETA*
@*(0.03590092383+ETA*(0.03742563713+ETA
@*0.01451196212)))-ELN*(0.5+ETA*(12498593597
@+ETA*(0.06880248576+ETA*(0.03328355346+ETA
@*0.00441787012))))

```

```

GOTO 20,
10 IER=1
20 RETURN
END

```

```

C*****
C
C SUBROUTINE :TEST
C - TEST THE LOCATION OF THE DROPLET. IF THE
C DROPLET IS OUTSIDE THE TUNNEL A WARNING MESSAGE WILL
C APPEARS.
C
C*****
C
C LIST OF VARIABLES :-
C RAD -RADIAL DISTANCE OF THE DROPLET FROM THE CENTRE
C XL -THE X CO-ORDINATE OF THE DROPLET
C Y(I) -THE ARRAY OF RADIUS FOR THE TUNNEL
C
C*****

```

```

SUBROUTINE TEST (XL,YL,ZL,X,Y,N1,IOU)
REAL X(N1),Y(N1),XL,YL,ZL,RAD

```

```

C SELECT THE FRUSTUM WHERE THE DROPLET IS LOCATED
C-----

```

```

      I=1
51 CONTINUE
      IF(XL .GT. X(I)) GOTO 50
      I=I+1
      GOTO 51
50 CONTINUE

```

```

C CALCULATE THE RADIAL DISTANCE OF THE DROPLET AND
C COMPARE IT WITH THE WITH THE RADIUS OF THE TUNNEL
C-----

```

```

      RAD=(YL*YL+ZL*ZL)**0.5
      IF(RAD .GT. Y(I)) GOTO 52
      GOTO 53
52 IOU=2
53 RETURN
END

```